A Quasi-Wavelet Function Basis for Improved Time-Frequency Characterizations

Yueon-Ron Lee
Institute of Harbor and Marine Technology

Email: ronlee@ms4.hinet.net

August 6, 1999

LIST OF CONTENTS

LIST OF FIGURES

LIST OF TABLES

ABSTRACT

A quasi-wavelet function basis with superior capability over the Morlet wavelet basis in extracting the power ridges of a signal is devised. Various simulated and experimental signals are used to validate the serviceability of this wavelet variant. Analytical aspects of the devised basis, such as frequency leakage-in and -out, ambiguity effects, phase noise, and the existence of local power minima, are studied and compared to the corresponding counterparts of Morlet wavelet; these characterizations manifest the usefulness of the wavelet variant basis for both modulus and phase renditions.

Chapter 1

Introduction

From time beginning of signal processing concerning the matching or simulation of intrinsic signal constituents, we are constantly pursuing function bases as well as their associated numerical processes that are not only precise but also easy and efficient. The fact is that there is not a common basis that is optimum for all applications, nor does it exist a general scheme that best appeals to all situations.

Both the windowed Fourier transform and the wavelet transform project a function into a certain function basis mainly for characterizing the non-stationary features of signals. In the former the basis is comprised of windowed Fourier eigenvectors; in the latter the basis is formed by wavelet atoms. Ideally, one would like to have a transform that does not spread signal energy in time and frequency. Or desirably, the transform should yield time-frequency distributions that have minimum ambiguity due to time and frequency spreading as well as least interferences among component signals (not necessarily Fourier components). However, due to the restriction of the Heisenberg uncertainty principle as well as the many lingering paradoxes (such as negative frequency, negative power, unallocated frequency components, etc.) of various time-frequency analyzing kernels, the ambiguity and the interferences can never be totally or simultaneously removed. There are always trade-offs among different bases and different approaches.

In the interest of providing an improved time-frequency analyzing kernel for those applications that mainly concern the continuous wavelet transform using the

Morlet wavelet function basis, the present study works on a new wavelet variant function basis and peruses its related characterizations.

Due to the inherent imperfection associated with the "quasi" nature of the proposed new "wavelet variant function", when characterizing the new basis, more emphases are placed on its practical usefulness in applications rather than its fulfillments of various constraints in analytical aspects. Nevertheless, we shall somewhat follow the formalism of time-frequency analysis in illustrating these shortcomings. And, if appropriate, explain why these shortcomings can still provide practical usefulness. Besides, such a process acquaints us with analytical countenance as well as applied demeanors and could possibly leads us to where efforts need to be made.

To show that the present tactic does provide easier and refined identifications of component ridges for a broad spectrum of signals, either from the modulus or phase perspectives of time-frequency characterizations, we put to tests various numerically simulated signals and laboratory water wave signals of both wind and mechanically generated waves.

Chapter 2

The Wavelet Variant

2.1 Introduction

The Morlet wavelet through the use of a continuous transform is the most often adopted wavelet methodology for water-wave related studies, where "physic" is the main focal point [18] (and possibly, also the case in other disciplines that emphasize the "total positivity and complete oscillation" of the wavelet and scaling function, respectively [3, 4, 14]) . Without exception, the extraction and interpretation of features from this transform coefficients are influenced by the uncertainties and interferences inherent to every time-frequency analyses as were mentioned in the introduction chapter.

In this chapter, with reference to the Morlet wavelet, we provide a quasi-wavelet seeding function, which, on the one hand, possesses the same easiness in numerical computation; one the other hand, holds an improved capability in extracting constituent components of a signal. That is to say, we will be working on a function basis that is capable of producing time-frequency planes that have smaller ambiguity effects (or frequency smearing) and also suffers lesser abstruseness from interferences of signal components.

2.2 The seeding function for the new quasi-wavelet basis

The seeding function $\psi(t)$ for the new function basis is provided as:

$$\psi(t) = \frac{1}{\pi^{\frac{1}{4}}} \left[\mathrm{sgn}(t) \sin \omega_0 t - i \cos \omega_0 t \right] e^{\frac{-t^2}{2}}, \tag{2.1}$$

where ω_0 is related to the modulation frequency of the counterpart Gabor transform (or windowed Fourier transform), $\mathrm{sgn}(t)$ is the sign function, the exponential stands for a Gaussian envelope, and the constant is just for the matching to the counterpart constant of the Morlet wavelet (and somewhat for a unit norm). The shape of this wavelet variant is shown in figure 2.1. It is given the name of a "quasi" mother wavelet (to be explained in the next chapter). Except a sign function this definition is basically quite similar to the simplified Morlet wavelet shown in figure 2.2.

The scaled and displaced versions of the wavelet is :

$$\psi_{a,b}(t) = \frac{1}{\sqrt{a}\pi^{\frac{1}{4}}} \left[\mathrm{sgn}(t) \sin \omega_0 \frac{t-b}{a} - i \cos \omega_0 \frac{t-b}{a} \right] e^{\frac{-\frac{t-b}{a}^2}{2}}, \tag{2.2}$$

where a is a scale parameter and b is the translation parameter. The $\frac{\omega_0}{a}$ has a physical meaning of a carrier frequency.

2.3 The renditions of time-frequency planes

For a complex wavelet transform there are basically two types of time-frequency renditions (may be expressed in 2- or 3-D): one refers to the modulus and the other refers to the phase of transform coefficients. Generally speaking, different transform categories or transforms using different bases might place different or unequal weights on modulus of phase representations (for those transforms that use orthonormal, bi-orthogonal, and semi-orthogonal wavelets, or wavelet packets [3, 6, 26, 21], there is only the modulus representation). But it will be shown that our proposed method yields somewhat equally useful information from both perspectives.

For our proposed wavelet variant (equation 2.1) we give the following possible definitions for the renditions of modulus and phase.

For a function $f(t)$, the modulus of the transform coefficient is defined either as

$$|\langle f(t), \mathbf{I_m}\psi(t)\rangle + i\mathbf{H}[\langle f(t), \mathbf{I_m}\psi(t)\rangle]|, \tag{2.3}$$

or as

$$|\langle f(t), \mathbf{R_e}\psi(t)\rangle + i\mathbf{H}[\langle f(t), \mathbf{R_e}\psi(t)\rangle]|, \tag{2.4}$$

where $\mathbf{R}$ and $\mathbf{I}$ represent real and imaginary part, respectively, and $\mathbf{H}$ represents the Hilbert transform. Note that the implementation of wavelet transform in individual definition is based on either real or imaginary part only.

The phase is defined as

$$\tan\frac{\mathbf{R_e}\langle f(t), \psi(t)\rangle}{\mathbf{I_m}\langle f(t), \psi(t)\rangle} + \left(\frac{\pi}{2} \quad \text{or} \quad 0\right), \tag{2.5}$$

or as

$$\tan\frac{\mathbf{I_e}\langle f(t), \psi(t)\rangle}{\mathbf{R_m}\langle f(t), \psi(t)\rangle} + \left(\frac{\pi}{2} \quad \text{or} \quad 0\right). \tag{2.6}$$

The difference of the two definitions and the presence of the optional constants will come to light when we discuss the properties of the transform in the next chapter; basically they act as a phase rotation and can be used to switch the pattern of significant features associated with either the power ridges or the time-frequency spreads.

The origins and implementations of these definitions will be explained in the next chapter too, where we also give more than practically needed considerations on various topics of time-frequency characterizations — since if we merely concern about their applications, then simply the physical portrayal of modulus and phase suffice to tell all that matter. Nonetheless, these additional efforts seem warranting because we are comparing the new basis with that of the Morlet wavelet (or Gabor's short-time Fourier transform), where systematical and analytical exploitations of time-frequency features are well established. Moreover, stepping through these details enhances our understanding of the intrinsic natures of various function bases and provide prospects for further investigations.

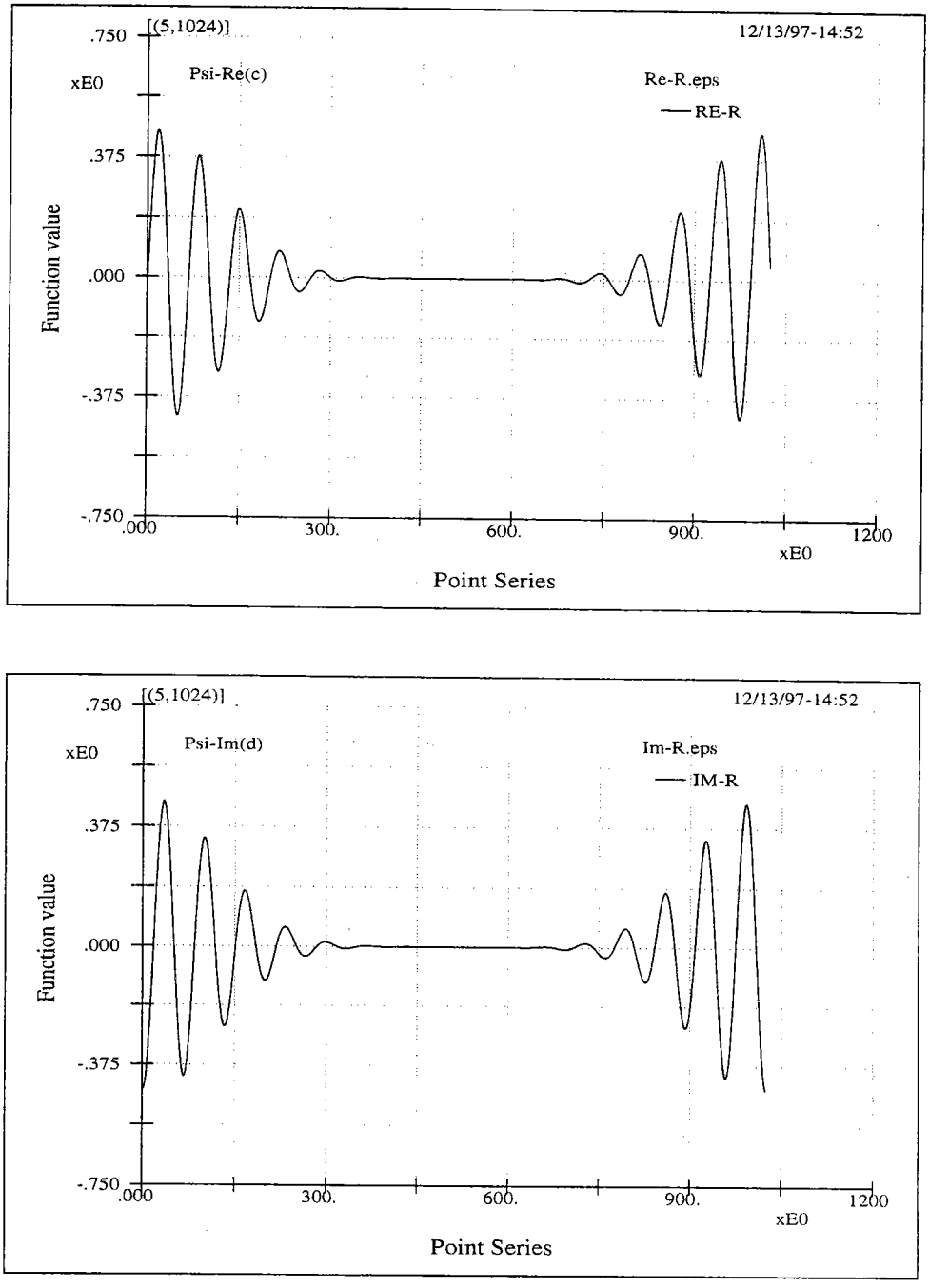

Figure 2.1: The real and imaginary parts of the quasi-wavelet for use in wavelet time-frequency renditions of modulus and phase as defined by equations 2.3, 2.4, 2.5 and 2.6. This wavelet is not analytic.

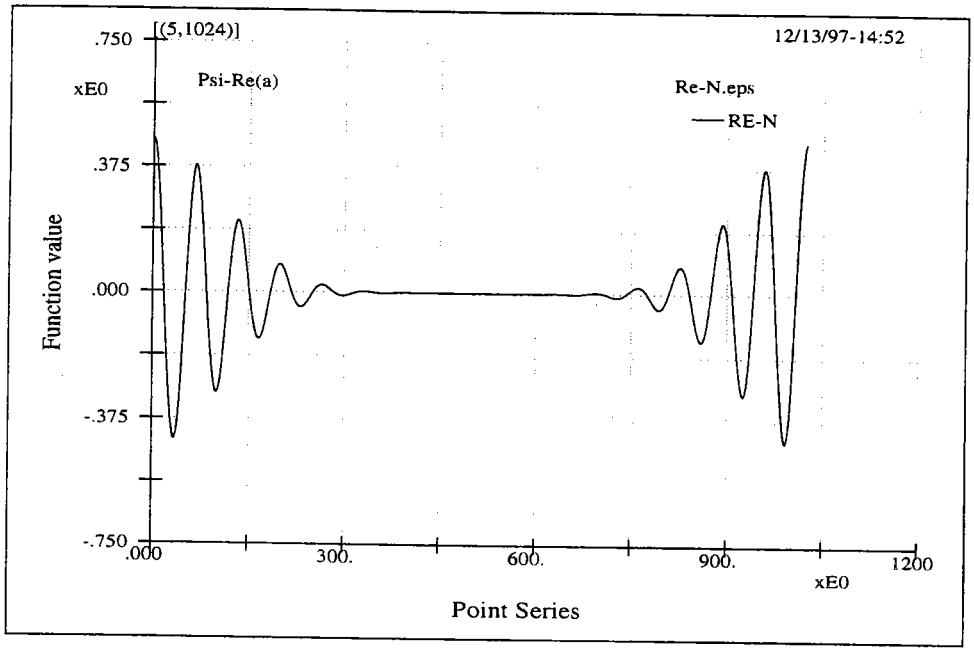

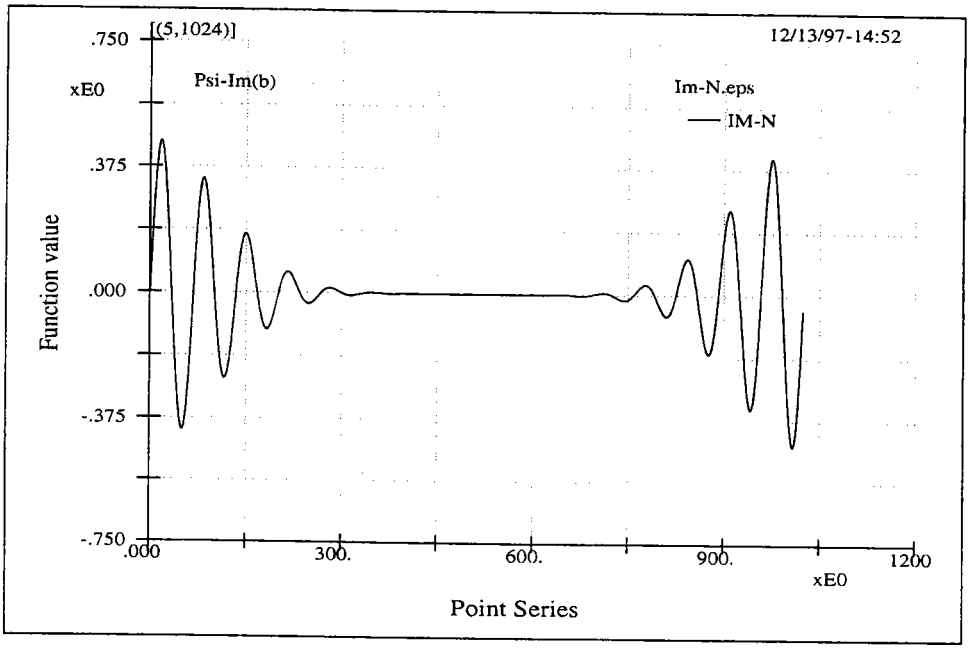

Figure 2.2: The real and imaginary parts of the Gabor type wavelet (the simplified form of Morlet wavelet) for use in the calculation of the first definition of modulus (equation 2.3). The wavelet is nearly analytic for most applications (when the carrier frequencies are not too low).

Chapter 3

Time-Frequency Characterizations

3.1 Introduction

A general class of time-frequency energy density decomposition is the Wigner-Ville distribution. The spectrogram of a windowed Fourier transform, the scalogram of a wavelet transform, and all squared time-frequency density distributions related to some inner products can all be associated with their specific forms of Wigner-Ville distribution [5, 22].

It is not known whether or not one can associate the proposed quasi-wavelet basis to a Wigner-Ville distribution (i.e., whether or not one can find the associated Wigner-Ville smoothing kernel or convolution operator for any L^2 function), but we are comparing its results to those of typical spectrogram and scalogram. Therefore, we shall more or less follow the formalism of time-frequency characterization so as to make contrasts for the various properties between the proposed quasi-wavelet function basis and that of the Morlet wavelet or Gabor transform. More specifically, the following topics will be considered:

- The wavelet admissibility condition as well as the concerns about the completeness, redundancy, and the stability of a transform;
- The analytic wavelet transform of a real signal and the wavelet transform of the analytic counterpart (which is complex) of a real signal;

- Concepts of time-frequency resolution, frequency leakage, and phase ambiguity;
- Local power maxima of an analytic windowed Fourier or wavelet transform versus local power minima associated with the use of the current wavelet variant. In particular, the phase and instantaneous frequency in association with an analytic signal (i.e, the relation between instantaneous frequencies and local ridge points of a scalogram or scalogram) versus the envelope or modulus of the wavelet variant transform;
- Phase "randomization" in association with an analytic transform versus phase "polarization" in association with the wavelet variant transform;

Elaborating on the above outlined items also helps to gain basic acquaintance of different basis categories, their distinct features, as well as individual advantages and disadvantages. This better prepares an intimate cognizance of the proposed basis function and provides possible prospects.

3.2 The admissibility condition and the completeness and redundancy

If a function $\psi(t)$ is to be qualified as a wavelet for the continuous wavelet transform (CWT), then the only requirement is that $\psi(t)$ meets the following "admissability condition",

$$2\pi \int_{-\infty}^{\infty} \frac{|\widehat{\psi}(\omega)|^2}{|\omega|} d\omega = C_\psi, \tag{3.1}$$

where C_ψ is a constant depending only on ψ only, and $\widehat{\psi}(\omega)$ is the Fourier transform of $\psi(t)$. Among the several definitions of the Fourier transform pairs the one adopted here is:

$$\widehat{\psi}(\omega) = \frac{1}{\sqrt{2\pi}} \int_{-\infty}^{\infty} \psi(t) e^{-i\omega t} dt \tag{3.2}$$

$$\psi(t) = \frac{1}{\sqrt{2\pi}} \int_{-\infty}^{\infty} \widehat{\psi}(\omega) e^{i\omega t} d\omega. \tag{3.3}$$

The admissability condition is the integration of power spectrum weighted by the inverse of the absolute value of frequency; therefore, to yield a finite value, the wavelet should have little power at low frequency and is totally nil at zero frequency, i.e., the area between the curve and the abscissa integrates to zero. This feature basically states that a wavelet should have reasonable decay or be finitely supported — so, it is a wave-let or a wavelet atom.

As to the origin of the constant C_ψ, it is a natural turnout of the derivation of the completeness (such as in the L^2 space) of the wavelet function basis, i.e., it is a byproduct when proofing the following "resolution of identity" for two functions g and h:

$$\langle g, h\rangle = \frac{1}{c_\psi}\int_0^\infty \frac{1}{a^2}\int_{-\infty}^{\infty}\langle g, \psi_{a,b}\rangle\overline{\langle h, \psi_{a,b}\rangle}dbda, \tag{3.4}$$

where $\psi_{a,b}(t) = \frac{1}{\sqrt{a}}\psi(\frac{t-b}{a})$ is a dilated and translated version of the mother wavelet $\psi(t)$ with dilation parameter $a > 0$ and $a \in \mathbf{R}$ and translation parameter $b \in \mathbf{R}$. The $\frac{1}{\sqrt{a}}$ is for the normalization of L^2-norm. The $\psi_{a,b}$ satisfies admissability condition too. In general, $\psi(t)$ is normalized such that $||\psi(t)|| = 1$; therefore, $\psi_{a,b}(t)$ also has a unit norm.

The admissability condition is a very loose constrain; it does not provide a clear concept of redundancy concerning applying CWT to either discretely sampled or continuous signals. To illustrate this redundancy, let us use the discrete wavelet frame (since the frame wavelet certainly qualifies as a wavelet for CWT): $\psi_{a_0,b_0;j,k}(t) = {a_0}^{-j/2}\psi({a_0}^{-j}t - kb_0)$, where a belongs to the set of discrete dilations a_0^j and b to the set of discrete translations $a_0^j kb_0$; $j, k \in \mathbf{Z}$; and $a_0 \neq 1$ and $b_0 > 0$ are fixed positive constants. For such a discrete wavelet frame we need to impose a more restrictive condition on $\psi(t)$ for its admittance, i.e., the stability condition,

$$b_0 A \leq 2\pi \sum_{j\in\mathbf{Z}} \left|\widehat{\psi}({a_0}^j\omega)\right|^2 \leq b_0 B, \tag{3.5}$$

where A and B are positive constants and $0 < A \leq B < \infty$. The fixed constants b_0 and 2π are intentionally kept since they are related to a normalized wavelet basis and since the magnitudes of A and B are related to the redundancy of the basis. The stability condition may look abstract, but we give its physical implication as: in order for a function to be reconstructed from its wavelet coefficients, i.e., the

operation is reversible, we need a process which is convergent when summing all its scales or frequency components. It is therefore necessary that the sum of the power of all the constituent elements can neither be nil or infinity. If the sum is zero, then the elements are all of zero measure — nothing exists. If the sum is infinity, then the elements are significantly overlapping in time and frequency — there is either too much dependence or too much ambiguity and tangling (just like two vectors paralleling to each other do not constitute a good vector basis in two dimensional vector space). If the basis functions are normalized and the inequality of the stability condition are optimized for both the greatest lower bound and the lowest upper bound, i.e., when A and B are defined as

$$A = \inf\left[\frac{2\pi}{b_0}\sum_{j\in\mathbf{Z}}\left|\widehat{\psi}(a_0{}^j\omega)\right|^2\right], \tag{3.6}$$

$$B = \sup\left[\frac{2\pi}{b_0}\sum_{j\in\mathbf{Z}}\left|\widehat{\psi}(a_0{}^j\omega)\right|^2\right], \tag{3.7}$$

then an indication of the redundancy is the average value of A and B, $\frac{A+B}{2}$, supposed that A and B are close to each other (almost tight). If $A = B = 1$, then the basis is orthonormal, and the transform coefficients are without redundancy. Based on this understanding we know that even a mother wavelet of an orthonormal Riesz basis will produce a redundant system when it is applied in the continuous sense. Therefore, continuous wavelet transforms are always redundant when applied to discrete signals and are complete when one likes to increase the resolution indefinitely.

Having stated so much, it is time to give the corresponding attributes of the proposed quasi-wavelet. If the real and imaginary parts of the quasi-wavelet is considered separatively, obviously neither integrates to a zero value. This implies that the formula for wavelet admissibility does not converge and therefore the function is really not a wavelet – This is the main reason why it is given the name of a "quasi"-wavelet. But in reality, both the real and imaginary parts do decay as exactly as those of the Morlet wavelet (again, more precisely, this should be the "quasi" equivalence or simplified version of the Morlet wavelet, or the Gabor type wavelet, as to be explained later). Therefore, practically we do not see any restraint

on its application; just as in almost all physical cases we use the simplified form of Morlet wavelet rather than its full legitimate form (to be stated later too).

In another perspective since the new basis function is "loose" in its categorization, i.e., it is neither a window Fourier transform nor a genuine wavelet transform, the trace of completeness and redundancy of its transform coefficients has also lost. However, from discrete (or finite resolution) point of view completeness and redundancy are more of theoretical interests rather than of practical value, especially when taking into account the fact that all signals embed uncertainty and all wave experiments involved uncontrollable or undesirable factors. In this regard, it has the same bearing as that of the Gabor type wavelet transform.

3.3 Transforms that lead naturally to ridge characterizations

In the following a good deal of attention is paid to the characterization of the Morlet wavelet. This is not only because we have mentioned it quite a lot of times but also because we are basically comparing the features of the proposed basis with those of the Morlet wavelet. Moreover, the Morlet wavelet play a unique dual role that no other function has — it crossovers the border between the continuous wavelet transform and the windowed Fourier transform. Due to this specific property, our perception of various characteristics of time-frequency analysis can be realized or threaded much more easily. Some of its significance in certain applications will also be stated in later sections (a more detail account was given in a previous report by the author [14]).

The Morlet wavelet is complex and is given by

$$\psi(t) = \frac{1}{\pi^{1/4}}(e^{-i\omega_0 t} - e^{-\omega_0^2/2})e^{-t^2/2}, \tag{3.8}$$

in which ω_0 is a constant and the term $e^{-\omega_0^2/2}$ justifies the admissability condition. Its Fourier transform is almost a shifted Gaussian and is given by

$$\widehat{\psi}(\omega) = \frac{1}{\pi^{1/4}}[e^{-(\omega-\omega_0)^2/2} - e^{-\omega^2/2}e^{-\omega_0^2/2}]. \tag{3.9}$$

The ω_0 is the modulation (or carrier) frequency and has the physical implication of the amplitude ratio r between the second highest peak and the highest peak of $\psi(t)$, i.e., $r = \psi(t_2)/\psi(0)$, in which t_2 is the abscissa of the second highest peak. The exact value of t_2 can be obtained by solving the transcendental equation numerically, but a fairly good explicit estimation is obtained by dropping the second term in the above equation since the second term is generally five order of magnitude less than the maximum value of the first term, i.e.,

$$\omega_0 \approx \frac{2\pi}{t_2} \approx \pi\left(-\frac{2}{\ln r}\right)^{1/2}. \tag{3.10}$$

The higher the ω_0 is, the smaller the ratio r becomes. If ω_0 is constant, then the ratio r for different wavelet dilations or scales keeps constant too.

By dropping the second term of equation 3.8 the $\psi(t)$ is strictly not a wavelet but more of a scaled windowed Fourier atom, and the transform becomes more of a scaled Gabor transform, i.e., the Gabor transform with additional scaling of its Gaussian window function. This basically states the dual role of the Morlet wavelet. From the point of view of discrete numerics, the two transforms might not use the same translation step. For the Gabor transform the step is in linear measure, and for the wavelet transform it is in logarithmic measure. Nevertheless, from a continuous perspective, the sense of translation step is trivial; therefore, they are basically identical except that, in the former, the shape and area of time-frequency windows are kept fixed; and, in the latter, the area is kept fixed but not the shape.

Based on the above understanding, there is a natural way to illustrate various wavelet ridge concepts using the scaled Gabor transform since it provides simple and clear illustrations through its intimate association with an analytic process and since the analytic procedure is earthy to the characterization of ridges. The following section describes these relations.

3.4 Analytic versus real function basis

We did not specifically mention in the above discussions that we had seemed to focus on complex basis functions. So, what is the point of using a complex basis when in reality there is no complex signal? An intuitive point for this is that the

sense of frequency can only be easily tackled by complex functions, which enable us to separate amplitude and phase. However, there is a deeper concern about the existence of negative frequencies since their occurrence retards our mental realization. But, the Fourier transform of a real signal is certainly with both positive and negative frequencies (so, the power spectrum is symmetrical). The desire to get round of the negative frequency of a transform lies the fundamental purpose of the use of an analytic basis.

There are two concepts here that are fundamentally significant. First, the Fourier transform of the product of two functions (such as a signal and a window function) is associated with a linear convolution operator, and a convolution in one domain corresponds to a multiplication in the other domain; therefore, if we can design a frequency window which only localized in the positive frequency and then multiplies the spectral results of the signal with this window then we might have the desire analytic signal. Second, since the frequency windows must not extend to the negative frequency, its center should lie away from the zero frequency. And since in Fourier transform a shift in one domain is equivalent to an oscillation in the other domain. Therefore, the analyzing atoms of the analytic function basis should have both reasonable oscillation and well regularity in its time domain such that they are band-limited (or almost band-limited) windows in the frequency domain.

These explanations lead us to a basic and important understanding: Why, up to the present time, for applications focusing on physics where positive frequency is important, the most useful and most often seen analyzing function bases are associated with a modulated Gaussian shape function – Since these basis functions satisfy the requirement of reasonable oscillation and are feasibly smooth [17, 14, 22].

With a phase it is natural to discuss the idea of instantaneous frequency. However, to the author's knowledge, in identifying instantaneous frequencies the modulus planes are ubiquitously used and the phase representations are almost rampantly entertaining. This is partly because phases do not differentiate the relative importance of individual components such that a phase plane is always fully occupied (this is well illustrated by the middle sub-figure of figure 3.1).

Here we shall illustrate three aspects based on the definitions given in the previous chapter. First, for a traditional analytic process, the instantaneous frequency is associated with the local energy peak, i.e., ridge point of modulus. Second, for

the new process, the instantaneous frequency is associated with the local energy trough. Third, our phase representation yields completely different but much informative picture as compared to the traditional one.

For the first two aspects, even though our definitions of time-frequency modulus plane involve the Hilbert transform, which is related to an analytic process, the analyzing function are not always analytic. Specifically, equation 2.3 yields nearly exactly the same results as those of Morlet wavelet, which is almost analytic and the instantaneous frequencies are associated with ridge points; equation 2.4 provides the new improved ridge extraction scheme, where the associated analytic signal is not quite clear. Moreover we shall see that equation 2.3 is associated with the power maxima, while equation 2.4 is for power minima.

For the third aspect, in addition to the fact that a time-frequency phase plane is certainly fully filled with phases no matter what the values of modulus are, we shall also illustrate that the phase values based on the Morlet transform are too extremely varying such that they could hardly show any feature of practical significance. While in contrast, our phase rendition yields almost polarized phase distribution where phases are mostly seated at or out of phase by convenient separation distances (such as $\pi/2$, π, $3\pi/2$ or 2π); furthermore, contrast interfaces occur at points of significant attributes such as minimum power points or transition points featuring time and frequency spreading (or time-frequency resolution).

3.5 Instantaneous frequencies and the ridge or trough points

The instantaneous frequency (or simply frequency) is generally defined as the time derivative of phase. Let suppose we have a real wavelet function basis, then we have two ways to derive the phases. One way is to devise an analytic wavelet function basis with real and imaginary parts as oppose to a basis of real functions only; another way is to convert first the real signal into an analytic counterpart signal and then apply a real function basis. It can be shown that the two approaches yield exactly the same result (see e.g., [22]).

The first definition of modulus, equation 2.3, is associated with an analytic function, and this function is almost the Morlet wavelet. As is seen from figure 3.1,

the Morlet wavelet, although, is not strictly without zero frequencies; it is nearly analytic. Here the figure shows the difference between the results derived from equation 2.3 and those derived from the Morlet wavelet, i.e., the difference between $\langle f(t), A[\psi] \rangle$ and $\langle f(t), \psi \rangle$, where $\psi(t)$ stands for the Morlet wavelet, A means finding the analytic counterpart, and the $f(t)$ is an X-signal (a signal composed of two linear chirps with a cross of frequency).

As to equation 2.4, the proposed quasi-wavelet is not analytic (there is no legitimate carrier) and might not be fully qualified as a seeding function for a complete set of basis functions; this is opposite to the cases of the Gabor or wavelet transform; therefore, the arguments related to local energy ridge do not apply. Rather we shall verify numerically that the current definition of equation 2.4 is associated with the lowest trough point located nearly at the instantaneous frequency as is derived from the analytic counterpart of the signal or an analytic wavelet transform.

Using the Mathematica programming language we numerically calculate the frequencies of the trough points to be $\frac{1}{0.969621}$ time the values of the ridge points associated with the Morlet wavelet. Here the ω_0 is taken as the commonly adopted value of 5, but different ω_0 yield values little different than 0.9696. It is also noted that in all comparison pairs (figures to be shown) the used parameters (such as adaptive values of ω_0 and integration limits) are the same.

As is clear from earlier statements, a function is analytic if we drop the negative frequency components of its Fourier transform. Conversely, an analytic function is necessary complex but is entirely characterized by its real part. If a real and symmetry window $g(t)$ is band-limited, than by applying a frequency modulation to the window one could possibly derive (subjected to the admissibility condition stated above) an analytical wavelet. Since equation 2.1 is not analytic, we take a different approach in the designs of its modulus representation. For the second definition (equation 2.4), the transform is performed on the real part only and then the analytic signal procedure is applied to this transform result, finally the envelope curve of the modulus is calculated accordingly.

In the following we give a brief description of the relation between the instantaneous frequency and the ridge point for an analytic signal (this applies to the first definition for modulus):

Let $g(t)$ be a window function which is centered around 0 and has unit norm

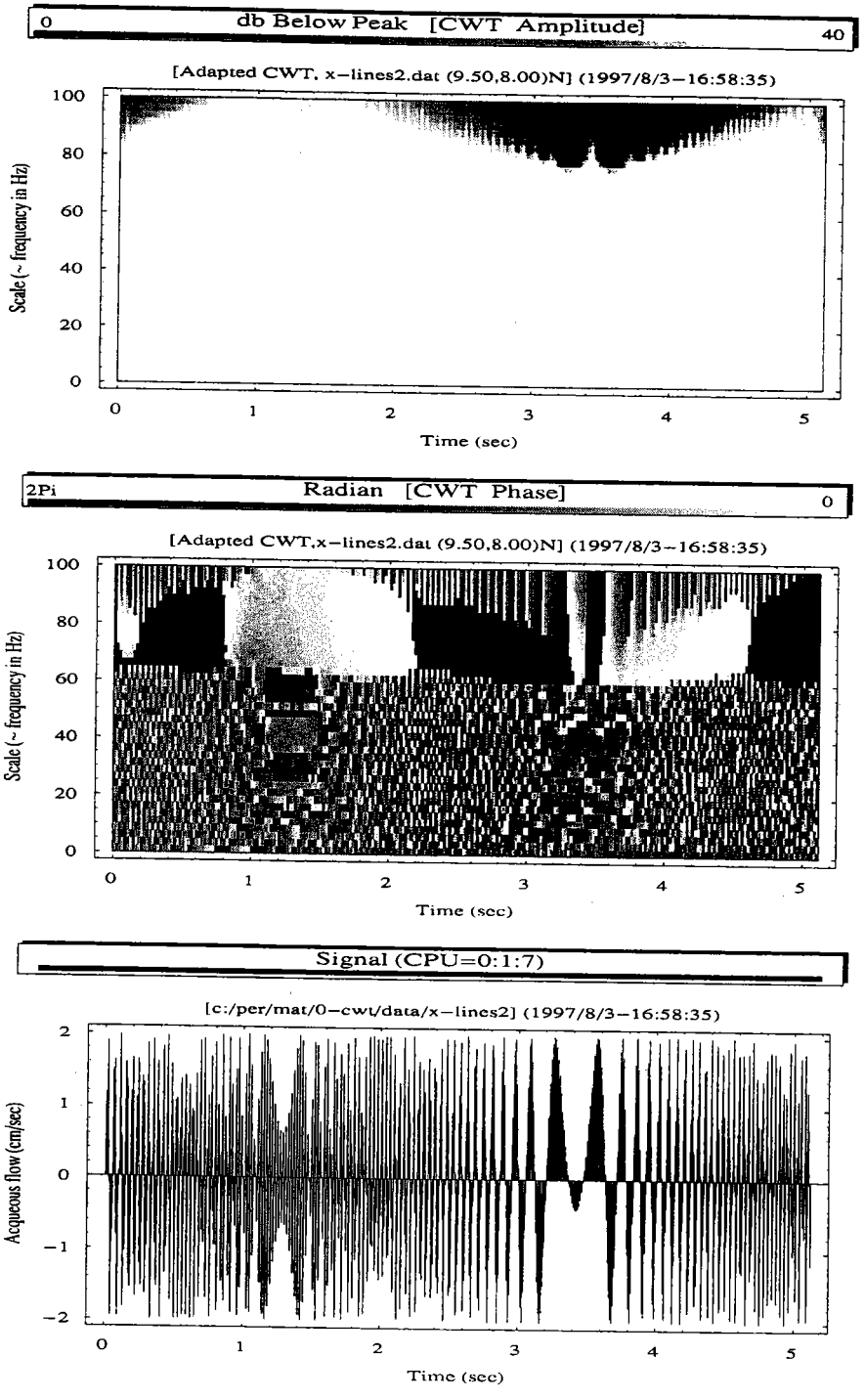

Figure 3.1: This figure shows how analytic the Morlet wavelet (simplified form) is, i.e., it shows the difference between $\langle f(t), A[\psi] \rangle$ and $\langle f(t), \psi \rangle$, where A means the analytic counterpart. Here an X-signal (composed of two linear chirps, see figure 4.6) is used.

with reasonable decay on its support (i.e., $\widehat{g}(0) = \int_{-\infty}^{\infty} g(t)dt$ is the maximum value of $\widehat{g}(\omega)$ and is of the order of 1). The windowed Fourier atom is

$$g_{u,\xi}(t) = g(t)e^{i\theta}. \tag{3.11}$$

The Fourier atom scaled by s is

$$g_{s,u,\xi}(t) = g_s(t)e^{i\theta}, \tag{3.12}$$

where $g_s = \frac{1}{\sqrt{s}}g(\frac{t}{s})$ has a support of $g(t)$ scaled by size s and is also with unit norm.

The scaled windowed Fourier transform (or the wavelet transform using the simplified Morlet wavelet, i.e, neglecting its second term) of a real function $f(t)$ is

$$\langle f, g_{s,u,\xi}\rangle = \int_{-\infty}^{\infty} f(t)g_s(t-u)e^{-i\xi t}dt. \tag{3.13}$$

Since any $f(t)$ can always be expressed as $f = a(t)\cos\phi(t)$, one has [28, 22]

$$\langle f, g_{s,u,\xi}\rangle = \frac{\sqrt{s}}{2}a(u)e^{i(\phi(u)-\xi u)}\left(\widehat{g}\left(s[\xi - \phi^{'}(u)]\right) + \epsilon(u,\xi)\right), \tag{3.14}$$

in which the ϵ is an overall corrective term determined by the following four elements:

- The relative variation of amplitude: $\epsilon_{a,1} \leq \frac{s|a^{'}(u)|}{|a(u)|}$;
- The relative curvature of amplitude: $\epsilon_{a,2} \leq \sup\frac{s^2|a^{''}(u)|}{|a(u)|}$;
- The rate of variation of frequency : $\epsilon_{\phi,2} \leq \sup s^2|\phi^{''}(t)|$; and
- The effects caused by the high frequency components of the window function, i.e., the extreme of the high end part of $|\widehat{g}(\omega)|$: $\epsilon_g = \sup_{|\omega|\geq s\phi^{'}(u)|}|\widehat{g}(\omega)|$

From the above descriptions we know that, to apply the ridge identification criterion of stationary phase (i.e., $\phi(u) - \xi u = 0$ or $\xi - \phi'(u) = 0$), the $f(t)$ (which can be viewed as a single component or combination of components) need to be relatively smooth. Considering that various time-frequency transforms are simply

implementing a projection mechanism such that we would like to have a set of transform coefficients that has a minimum entropy [29, 30] (i.e., matching signal components with the basis functions), We further understand why it is practically important that the wavelet should be completely oscillating and the scaling function should be totally positive [4, 16, 15] – With these properties the basis functions also possess the various small corrective terms listed above.

One more point to note is that even though individual components follow the above restrictions, the combination of components might not follow the restrictions if there are interferences among components. Therefore, an entirely different class of function basis (i.e., neither a windowed Fourier basis nor a wavelet basis) might possibly avoid or be less influenced by these restrictions. Incidentally, the proposed quasi-wavelet basis is luckily the one.

In the following section we focus on how to handle the analytic procedure; this in turn deals with the Hilbert transform.

3.6 The analytic signal procedure and the Hilbert trans form

Having stated the usefulness of an analytic signal or analytic function basis in power ridge extraction in association with the Gabor transform and Morlet wavelet transform, we now work on what are involved in an analytic procedure that aims at finding the analytic counterpart of a function. It will be clear that such a procedure inherently involves the Hilbert transform.

Another direct relevance of this section to the present study is the used of the Hilbert transform in equations 2.3 and 2.4, even though the perspective now is not on the relation between instantaneous frequency and the ridge point (since the quasi-wavelet does not meet the basic assumption of being a well band-limited function, as is the case for a Gaussian wavelet atom; nor is the proposed quasi-wavelet analytic). Therefore, it warrants for us to work through the details that lead to a very easy implementation of the Hilbert transform. This also helps to illustrate possible difficulties or uncertainties that quite often induce paradoxes due to non-conformance to the above listed constraints.

Let a real signal be $f_r(t)$ and its sensible imaginary counterpart be $f_i(t)$. The

real and imaginary parts form a complex signal $z(t)$. A complex function allows us to define its amplitude (or modulus) function $a(t)$ and phase function $\phi(t)$ of the complex exponential. The derivative of the phase yields the natural definition of instantaneous frequency (or local wavenumber in spatial domain) $\omega_i(t)$. The simple mathematical form is

$$z(t) = f_r(t) + f_i(t) = a(t)e^{i\phi(t)}, \tag{3.15}$$

with

$$\omega_i(t) = \phi'(t). \tag{3.16}$$

The main concern here is what is the sensible imaginary part since its choice affects our exploitation of instantaneous frequency. It is appropriate to point out that in the realm of signal analysis most researchers still view the instantaneous frequency as merely a primitive concept rather than a question of mathematical definition. That is to say, the proper definition of the complex signal is still regarded as an open question [5]. And the issues are, at best, whether a particular definition can match our intuitive thinking; whether its results can provide adequate explanations for the physics that might be of our own logical reasoning only; or whether the intuitive assumptions induce additional concerns which might be counterintuitive and possibly bring us to new discoveries.

Since any real signal $f_r(t)$ can be expressed as

$$f_r(t) = a(t)\cos\phi(t), \tag{3.17}$$

The most intuitive realization of the complex signal $z(t)$ should be

$$z(t) = a(t)e^{i\phi(t)}. \tag{3.18}$$

Nevertheless, there are infinitely many ways to devise such a complex form. This reflects the openness of the definition of the instantaneous frequency.

In 1946 Gabor [7] proposed a definition for the complex signal that is unique for any real signal and his method is generally referred as the analytic signal procedure.

Let $F_r(\omega)$ be the Fourier transform of $f_r(t)$, the corresponding analytic signal

Gabor introduced is,

$$z(t) = 2\frac{1}{\sqrt{2\pi}}\int_0^\infty F_r(\omega)e^{i\omega t}d\omega, \tag{3.19}$$

where the factor 2 is introduced so that the real part of the complex signal is equal to the original signal. As is clear from the basic properties of Fourier transform, $z(t)$ must be complex and is the inverse Fourier transform of a single-sided spectrum, which drops the negative frequency components but keeps the same positive spectral components as those of $F_r(\omega)$. Obviously, when the Fourier transform is applied to $z(t)$ again one gets only positive frequency constituents.

Next we illustrate how such a simple complex function can be used to calculate the Hilbert transform of $f_r(t)$. And, in fact, the Hilbert transform is the imaginary part of $z(t)$.

That is to say, we should verify the following identity [5]:

$$z(t) = f_r(t) + i\frac{1}{\pi}\mathcal{P}\int_{-\infty}^{\infty}\frac{f_r(\tau)}{t-\tau}d\tau, \tag{3.20}$$

in which the Hilbert transform of the signal, $\mathcal{H}[f_r(t)]$ is

$$\mathcal{H}[f_r(t)] = \widetilde{f_r(t)} = \frac{1}{\pi}\mathcal{P}\int_{-\infty}^{\infty}\frac{f_r(\tau)}{t-\tau}d\tau. \tag{3.21}$$

In the equation the symbol $\mathcal{P}$ means that the integration is carried out based on the rule of Cauchy principal value, i.e.,

$$\mathcal{P}\int = \lim_{\epsilon_1=\epsilon_2\to 0}\left(\int_{-\infty}^{t-\epsilon_1} + \int_{t+\epsilon_2}^{\infty}\right). \tag{3.22}$$

Let

$$g(t) = \frac{1}{t}, \tag{3.23}$$

then the Hilbert transform is simply the convolution of $f_r(t)$ and $g(t)$, i.e.,

$$\widetilde{f_r(t)} = \frac{1}{\pi}(f_r \star g)(t). \tag{3.24}$$

By the Fourier duality property, the Fourier transform of the convolution is

$$\mathcal{F}[\widetilde{f_r(t)}] = \widehat{H}(\omega) = \frac{1}{\pi} F_r(\omega) G(\omega). \tag{3.25}$$

Now with $F_r(\omega)$ and $G(\omega)$ being separated the Cauchy principal value operation is related to $g(t)$ only. And the Fourier transform of g is

$$\mathcal{F}[g(t)] = G(\omega) = \mathcal{P} \int_{-\infty}^{\infty} \frac{e^{-i\omega t}}{t} dt =$$
$$\mathcal{P} \int_{-\infty}^{\infty} \frac{\cos(\omega t)}{t} dt - i \int_{-\infty}^{\infty} \frac{\sin(\omega t)}{t} dt. \tag{3.26}$$

Since the integrant associated with the real part of this equation is antisymmetry the Cauchy principal value integration of this part is zero. As to the integration of the imaginary part, since $\frac{\sin(\omega x)}{x}$ is finite for all values of x, including $x = 0$, there is no need of the principal value sign. Of this part, the integrant is symmetrical; therefore, only half of the integration needs to be considered, and through a change of variable one gets

$$\int_0^{\infty} \frac{\sin \omega x}{x} dx = \mathrm{sgn}(\omega) \int_0^{\infty} \frac{\sin u}{u} du. \tag{3.27}$$

Here one basically know that $G(\omega)$ does not depend on the variation of ω since the integration is independent of ω. Though this integral looks simple, its integration should not be treated as a trivial process; rather, a closed form of the integration can be derived through the use the residue theorem of integration from the complex integral calculus (see for example the well written textbook by Greenberg [8]). The final result is a simple relation which only depends on the sign of ω:

$$G(\omega) = \begin{cases} -i\pi \mathrm{sgn}(\omega) & \omega \neq 0 \\ 0 & \omega = 0. \end{cases} \tag{3.28}$$

Accordingly, the Fourier transform of the analytic signal $\mathcal{A}[f_r(t)]$ is

$$\mathcal{F}[\mathcal{A}[f(t)]] = F_r(\omega) + i\mathcal{F}[\mathcal{H}[f_r(t)]](\omega) = \begin{cases} 2S(\omega) & \omega > 0 \\ 0 & \omega \leq 0. \end{cases} \tag{3.29}$$

Here we see that this equation matches exactly with equations 3.19 and 3.20 combined. And it further yields

$$\widehat{H}(\omega) = \begin{cases} -iF(\omega) & \omega > 0 \\ iF(\omega) & \omega \leq 0. \end{cases} \tag{3.30}$$

Making use of this relation the Hilbert transform is easily implemented by a simple word (subroutine) in ASYST language as is shown in Table 3.1.

Detail manipulation of the analytic signal approach is given here not merely for its analytical interest, but rather to disclose its intrinsic nature in association with the Fourier transform properties. An alternative approach implemented in the time domain based on Parks-McClellan minimax algorithm was given in an earlier report on characterizing the amplitude and frequency modulations of water waves measured in laboratory wave tank experiments [13]. In which trade-offs between the two implementations were also illustrated. Here we add one point to the statement given in the introduction chapter – that any numerical scheme is hardly optimum.

As is also indicated in the program one needs to exercise cautions related to non-stationary effects since the basic tactic is related to several simple processes that only manipulate the contents of the FFT of the input signal. And, additionally, we must also acknowledge that the standard deviation of a spectrum is rather significant and its refinement is quite demanding concerning the amount of data points required.

Overall, here we further illustrate that the ridge algorithm of a Gabor type wavelet transform is only true when the various restraints listed in section 3.5 are obeyed. In analytical term, if we regard the inner product of the transform of equation 3.14 as a linear operator L, then L must be of a weak continuity, i.e., $Lf(t)$ is modified by a small amount if $f(t)$ is only slightly modified. Thorough numerical experiments on this using laboratory wave data fully support these arguments as are detailed by a previous report by the author [14] (which also includes refined statements of two earlier related papers [16, 15]).

In reality, the above elaborations further manifest an important realization — Due to the fact that the operations associated with an orthonormal transform or any efficient transform are not in weak form, orthonormal function bases just do not provide as informative physics as what can be provided by the continuous wavelet

transform using the Morlet wavelet – Redundancy is sometimes quite helpful [23, 14, 18].

Let us recap the scheme for the definition of equation 2.4. Rather than converting the signal into its analytic counterpart and then projecting it into a real wavelet basis, or rather than directly projecting the real signal into an analytic wavelet basis, the signal is first projected into the real part of the wavelet basis and then the analytic signal procedure is applied to the transform coefficients. In this way the time-frequency energy density distribution is obtained as the envelop of the real part wavelet coefficients, i.e., the modulus of the complex transform coefficients.

3.7 Time-frequency resolution, frequency leakage, and phase ambiguity

Conventional time-frequency resolution measures a basis atom's spreads in time and frequency. If time and frequency distances between component signals are too short and the overlapping of their energy is significant, or component signal's power is overshadowed by others', then the identification of component signals is difficult.

Since a function can not be finitely supported both in time and frequency domains, there is no precise time-frequency resolution; rather, we generally use the second central moments in time and frequency of the basis atom to represent its spreads or resolutions.

For the Morlet wavelet the wavelet atom is of a modulated Gaussian which has an envelope centered and peaked at zero time, and the atom has an exact carrier frequency. For the wavelet variant the envelope can be treated as either a singly peaked bump (the same Gaussian envelope) or a bump with double peaks (Gaussian envelope with a shift of peak of $\pm\pi/2$ so as to match the peaks of envelope to the top points of the oscillation curve), but the atom does not have a carrier frequency; nevertheless the waveform does have an oscillation parameter that is derived from the carrier frequency of the Gabor transform.

Therefore, although it is fully legitimate to use time-frequency resolution windows to study the smearing effects for the Morlet wavelet, it is more appropriate

Table 3.1: An ASYST word (equivalent to a subroutine in some computer languages) that calculates the Hilbert transform of a signal. The word takes a one dimensional array as the input argument. As seen from the programming, the basic tactic is related to several processes manipulating the contents of the FFT of the input signal. It is of no doubt that these processes inscribe the properties related to FFT into the results of the analytic signal. This is based on the understanding that the standard deviation of a spectrum is rather significant and its refinement is quite demanding concerning the amount of data points required. Alternatively, we practically illustrate that the ridge algorithm of a Gabor type wavelet transform is only true when the constraints listed in section 3.5 are obeyed.

```
\ ------------------------------------------------------------------------
\  A small program piece which finds the imaginary part of a real signal
\     based on the analytic signal procedure.
\  The computation makes use of the final results of complex calculus based
\     on Cauchy principal value integration.
\  The length of the input array will be automatically truncated to the
\     maximum allowable power of 2.
\ ------------------------------------------------------------------------
: my.hilbert
  fft   []size   n.fft.pts  :=
  dup   becomes>  t1

  dup   sub[ 1 , n.fft.pts  2  /  ]
  0     +1     z=x+iy   *
  t1    sub[ 1 , n.fft.pts  2  /  ]  :=

        sub[ n.fft.pts  2  /  1 +   ,  n.fft.pts  2 / ]
  0     -1     z=x+iy   *
  t1    sub[ n.fft.pts  2  /  1 +   ,  n.fft.pts  2 / ]  :=

  t1    ifft
  zreal
;
\ ------------------------------------------------------------------------
```

to discuss in terms of time and frequency leakages for the current wavelet variant, as will be clear form the bumps of the figures shown later. But still, it is equally legitimate to discuss time and frequency leakages for the Morlet wavelet.

For frequency leakage-out we mean the smearing brought by a unit scale wavelet to its neighboring wave packets of various scales; conversely, there is a frequency leakage-in which is induced by a neighboring scale. Note that here we use the term "scale" rather that "frequency", this is to emphasize that we are projecting wave packet (rather than a constant sinusoidal wave) into the wavelet atom.

For time smearing we mean the ambiguity caused by the phase mismatch between a wave packet and the wavelet atom. That is to say, it is calculated by projecting a wave packet into a time-translated wavelet atom.

The Mathematica programming language is used to shed light on these arguments. Its program is appended at the end of this chapter. The algorithms are somewhat self-explained in the program.

Let us list a few important characterizations from the results:

- For the present wavelet variant the closed form representation for the leakage-out is derived as

$$
\begin{aligned}
P(a,\omega_0) \;=\; & \frac{1}{\left(\frac{\left(\frac{1}{a}\right)^2+1}{\omega_0^2}\right)^{0.5}}\left(\frac{1}{2}\left(\sqrt{\frac{\left(1+\frac{1}{a}\right)^2\omega_0^2}{\left(\frac{1}{a}\right)^2+1}}\times\right.\right. \\
& {}_1F_1\left(1;\frac{3}{2};-\frac{\left(1+\frac{1}{a}\right)^2\omega_0^2}{2\left(\left(\frac{1}{a}\right)^2+1\right)}\right)\operatorname{sgn}\left(1+\frac{1}{a}\right)+ \\
& \sqrt{\frac{(a-1)^2\omega_0^2}{\left(\left(\frac{1}{a}\right)^2+1\right)a^2}}\times \\
& \left.\left.{}_1F_1\left(1;\frac{3}{2};-\frac{(a-1)^2\omega_0^2}{2\left(\left(\frac{1}{a}\right)^2+1\right)a^2}\right)\operatorname{sgn}\left(1-\frac{1}{a}\right)+\right)\right) \qquad (3.31)
\end{aligned}
$$

in which a is a scale, ω_0 stands for a carrier frequency (in Morlet wavelet's term), and the ${}_1F_1$ stands for a hypergeometric function. For $\omega_0 = 5$ the frequency leakage-out has a root (i.e., zero value point) at scale 0.969621. For the Morlet wavelet the maximum leakage-out is locates at its own scale,

i.e., the self projection scale 1.

- For the wavelet variant the two sides of the zero value point have sharp steep slopes (when taking the modulus of the transform coefficient). Whereas, the Morlet wavelet is associated with a peak with a zero derivative, and around the peak the values are not in good contrast. Now it is clear that the most significant feature for the wavelet variant is caused by the existence of zero value modulus as well as the wherefore induced sharp contrast when comparing any neighboring value with a zero one (a non-zero number divided by zero is infinity).

- For the wavelet variant the energy leakage distribution of a wave packet has two bumps at opposite sides of the root point; while the Morlet wavelet has a single solid envelope. This explains why we use time and frequency leakages rather than resolution windows in discussing the discriminating capability of these wavelet atoms.

- A leakage-in curve is also shown which gives consistent results to those of the leakage-out. Note that here the values are not modified by the corresponding scale factors.

- The smearing (or contamination) of energy in time domain is calculated by projecting a shifted wave packet into the wavelet atom. This kind of leakage has the same meaning as the phase noise. Again, we have the same characterizations as the previous items — there is a root point at the zero phase point, and the modulus is also doubly peaked at the two sides of the zero phase point. Overall, the ridge of maximum power is for the Morlet wavelet, and its position corresponds (albeit the need of a multiplication factor of about $\frac{1}{0.9696}$ for scale adjustment) to the bottom point of trough of zero power for the present wavelet variant.

- Since at the bottom of the energy trough one of the real and imaginary parts is of zero value (depending on the choice of a datum), and since the leakage are always in opposite signs with respect to the root point, furthermore since there is a reflection point at each side of the leakage curve — the various time-frequency featuring points have phase values located at convenient

separation distances, and different visual patterns might show up through the rotation of phase or by adding a phase datum. These specific properties make possible the un-matchable characterizations of time-frequency features using the wavelet variant's phase plane.

Figure 3.2: (Shown as the first figure in the program) Frequency leakage-out of the wavelet variant. The frequency leakage-out is the projection of a wave packet of a certain scale (abscissa) into the unit scale wavelet atom. The root of the curve is 0.969621 for $\omega_0 = 5$. The zero value and sharp contrast around the root make possible the wavelet variant's successful applications.

Figure 3.3: (Shown as the second figure in the program) Frequency leakage-out of the Morlet wavelet variant. It lacks the benefit of a sharp contrast around the ridge points.

Figure 3.4: (Shown as the third figure in the program) Frequency leakage-in of the wavelet variant. The frequency leakage-in is the projection of a wavelet atom of certain scale (abscissa) into a wave packet of unit scale. It shows consistent results with the frequency leakage-out (in contrast to leakage-out, here the value is not modified by the corresponding scale).

Figure 3.5: (Shown as the fourth figure in the program) Phase noise of the wavelet variant. The phase noise is the projection of a translated wave packet of unit scale into the unit scale wavelet atom. There is a root at the zero phase. Again, the zero value and sharp contrast around the root constitute the other half of the reasons for the wavelet variant's successful applications.

Figure 3.6: (Shown as the fifth figure in the program) Phase noise of the Morlet wavelet. The phase noise is the projection of a translated wave packet of unit scale into the unit scale wavelet atom. There is a peak at the zero phase. Again, the zero derivative peak is not a good location for a phase identification.

(* A Wavelet Variant for Refined Ridge Extraction *)

(* by Ron Lee *)

Files and Parameters

File | Macro | LeakOut | LeakIn | PhaseNoise | Root | Others | End

```
<< "c:/lee/mat/SetNotebook_nbm.m" (* Set notebook options *)
<< "c:/lee/mat/run-form.miw";
<< "c:/lee/mat/fig-fram_nb-m.m";
<< "c:/lee/mat/000-word_nb-m.m";
myfont = "Times";
$TextStyle = {FontFamily -> "Times", FontSize -> myfontsize};
timeflag = "Y";
dynamictimeflag = "N";
flabelflag = "Y";
flabelflag2 = "Y";
abcdflag = "N";
llabelflag = "y";
gridlineflag = "YY";
xyaxisflag = "LL";
stringposflag = 1;
xshiftflag = 0;
forcedstringaryflag = "n";
```

Macros

File | Macro | LeakOut | LeakIn | PhaseNoise | Root | Others | End

```
doshowxy := {
  moutt[flabel];
  moutt[flabel2];
  myplot=ListPlot[ dataxy
    , PlotJoined->True
    , PlotRange->All
    , PlotStyle->{Thickness[0.0008] (* , Hue[0.0] *) }
    , Frame->True
    , DisplayFunction->Identity
  ];
  myshow;
  (* Run["mmawav.bat"]; *)
```

```
  <<"c:/lee/mat/000-p2_nb-m.m"
};
```

```
flabel2 := typestr<>"α="<>StringTake[ToString[N[scap1, 9]],If[StringLength[
ToString[N[scap1, 9]]]>=7, 7, 1] ]<>", β="<>ToString[N[
peakshiftp1,2]]<>"π, ξ="<>StringTake[
ToString[N[xi,2]],1]<>", (0↔"<>StringTake[ToString[N[xlimitp1, 2]],1]<>"π),
θ="<>ToString[N[phap1,3]]<>"π";
```

■ **Leakage out (Wavelet variant)**

```
(* --------- Frequency Leakage Out (Variant) ---------- *)
typestr="Wavelet Variant: ";
xlabel="Scale";
ylabel="Projections at different wavelet scales";
flabel="Ambiguity Effects : Leakage OUT from a wave packet";
<<"c:/lee/mat/000-p1_nb-m.m";
frelkgout [peakshiftv_, scav_, xlimitv_, phav_, xiv_] :=
  1 / (scav) * NIntegrate[Cos[xiv*x]*Sin[xiv*x/scav]*
     Exp[-((x - peakshiftv/xiv)^2/scav^2 - (x)^2)/(2)],
     {x, 0, xlimitv}
  , MinRecursion->3, MaxRecursion->10
];
  (*  1 / scav * NIntegrate[Cos[x]*Sin[xiv * x/scav]*   (* a=sca/xi *)
       Exp[-((x/scav - peakshiftv/xiv )^2 + (x)^2)/(2)],
  *)
peakshiftp1=0.5;peakshift= peakshiftp1 * Pi;
xlimitp1=7;xlimit=xlimitp1 * Pi;
phap1=0;pha=phap1 * Pi;
xi=5;
scap1=1;
datax= Table[ ni , {ni, 0.025, 5, 0.025}];
datay= Table[ frelkgout [peakshift, sca, xlimit, pha, xi], {sca, 0.025 ,
5 , 0.025 } ];
dataxy=Table[ {datax[[ i ]], datay[[i]]}, {i,1 ,Length[datax]}];
doshowxy;
```

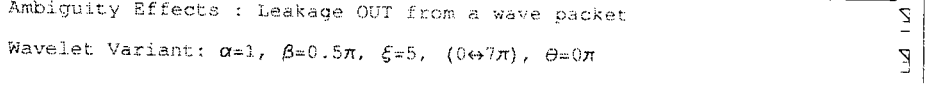

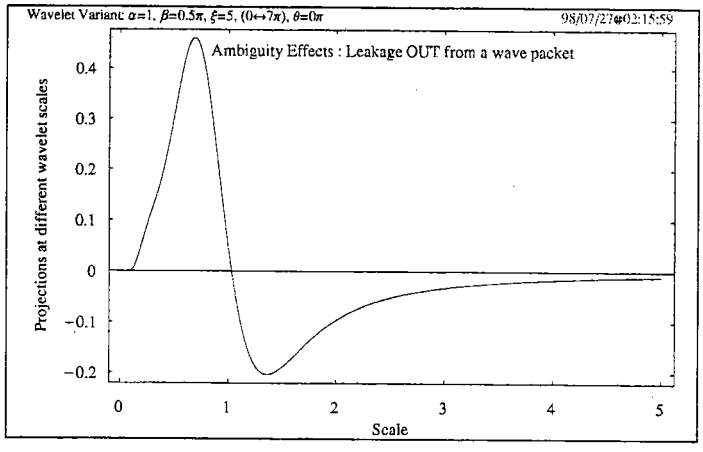


```
{1998, 7, 27, 2, 16, 0}    CPU:(00, 00, 40.04);    Time:(00, 00, 40)
```

■ Leakage out (Morlet)

```
(* --------- Frequency Leakage Out (Morlet) ---------- *)
typestr="Morlet Wavelet: ";
xlabel="Scale";
ylabel="Projections at different wavelet scales";
flabel="Ambiguity Effects : Leakage OUT from a wave packet";
<<"c:/lee/mat/000-pl_nb-m.m";
(*
frelkginM[peakshiftv_, scav_, xlimitv_, phav_, xiv_] :=
   NIntegrate[Cos[u/scav]*Cos[(u)]*
     Exp[-((u - peakshiftv)^2+ (u/scav)^2)/(2*xiv^2)],
     {u, 0, xlimitv}
     , MinRecursion->3, MaxRecursion->10
];
*)
(*  There exists analytical form  *)
frelkgoutM [peakshiftv_, scav_, xlimitv_, phav_, xiv_] :=
  2*  1 / (scav) * Integrate[Cos[xiv*x]*Cos[xiv*x/scav]*
     Exp[-((x - peakshiftv/xiv)^2/scav^2 + (x)^2)/(2)],
     {x, 0, Infinity}
];
peakshiftpl=0;  peakshift= peakshiftpl * Pi;
xlimitpl=7;  xlimit=xlimitpl * Pi;
phapl=0;  pha=phapl * Pi;
xi=5;
scapl=1;
dofrelkgoutM=frelkgoutM [peakshift, sca, xlimit, pha, xi](*analytical form*)

datax= Table[ ni , {ni, 0.000, 5, 0.025}];
datay= Table[ N[dofrelkgoutM], {sca, 0.000 , 5 , 0.025 } ];
dataxy=Table[ {datax[[ i ]], datay[[i]]}, {i,1 ,Length[datax]}];
doshowxy;
```

$$\frac{1}{sca}\left(2\,If\left[Im\left[\frac{1}{sca}\right]==0\;\&\&\;Re\left[\frac{1}{sca^2}\right]>-1\;\&\&\;Re\left[\frac{1+sca^2}{sca^2}\right]>0,\right.\right.$$

$$\left.\left.\frac{\left(E^{-\frac{25(-1+sca)^2}{2(1+sca^2)}}+E^{-\frac{25(1+sca)^2}{2(1+sca^2)}}\right)\sqrt{\frac{\pi}{2}}\sqrt{1+\frac{1}{sca^2}}\;sca^2}{2(1+sca^2)},\int_0^\infty E^{\frac{1}{2}\left(-x^2-\frac{x^2}{sca^2}\right)}\,Cos[5x]\,Cos\left[\frac{5x}{sca}\right]dx\right]\right)$$

Ambiguity Effects : Leakage OUT from a wave packet

Morlet Wavelet: $\alpha=1$, $\beta=0\pi$, $\xi=5$, $(0\leftrightarrow 7\pi)$, $\theta=0\pi$

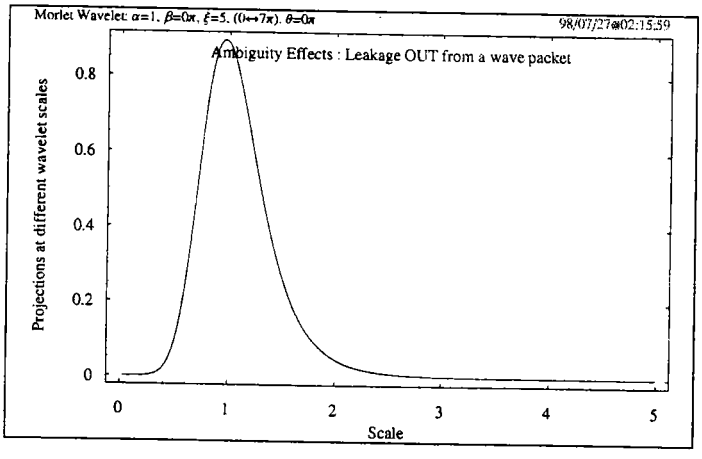

Graphics::gptn :
Coordinate ComplexInfinity in {0., ComplexInfinity} is not a floating-point number.

{1998, 7, 27, 2, 16, 40} CPU:(00, 00, 8.23); Time:(00, 00, 08)

■ `<< "c:\\lee\\mat\\000-p1.m";`

```
FindMinimum[-1 * 1 / sca *
  ((E^(-25 (-1+sca)^2/(2 (1+sca^2))) + E^(-25 (1+sca)^2/(2 (1+sca^2)))) Sqrt[Pi/2] Sqrt[1 + 1/sca^2] sca^2)/(2 (1 + sca^2)), {sca, 0.97}]
```

`<< "c:/lee/mat/000-p2_nb-m.m"`

{-0.447397, {sca → 0.962224}}

```
{1998, 7, 27, 2, 16, 48}    CPU:(00, 00, 0.05);    Time:(00, 00, 00)
```

Leakage In | File | Macro | LeakOut | LeakIn | PhaseNoise | Root | Other | End

■ Leakage in (Wavelet variant)

```
(* -------- Frequency Leakage In (Variant) -------- *)
typestr="Wavelet Variant: ";
xlabel="Scale";
ylabel="Projections from wave packets of different scales";
flabel="Ambiguity Effects : Leakage IN from different wave packets";
<<"c:/lee/mat/000-p1_nb-m.m";
frelkgin[peakshiftv_, scav_, xlimitv_, phav_, xiv_] :=
   NIntegrate[Cos[u/scav]*Sin[(u)]*
     Exp[-((u - peakshiftv)^2+ (u/scav)^2)/(2*xiv^2)],
     {u, 0, xlimitv}
     , MinRecursion->3, MaxRecursion->10
];
(* gsca[b_, a_, s_] := NIntegrate[Cos[u/a]*Sin[(u)]*
                 Exp[-((u-Pi/2.)^2.+(u/a)^2.)/(2*s^2)], {u, 0, b} ] *)
peakshiftp1=0.5;peakshift= peakshiftp1 * Pi;
xlimitp1=7;xlimit=xlimitp1 * Pi;
phap1=0;pha=phap1 * Pi;
xi=5;
scap1=1;
datax= Table[ ni , {ni, 0.025, 5, 0.025}];
datay= Table[ frelkgin [peakshift, sca, xlimit, pha, xi], {sca, 0.025 ,
5 , 0.025 } ];
dataxy=Table[ {datax[[ i ]], datay[[i]]}, {i,1 ,Length[datax]}];
doshowxy;
```

```
Ambiguity Effects : Leakage IN from different wave packets
```

```
Wavelet Variant: α=1, β=0.5π, ξ=5, (0↔7π), Θ=0π
```

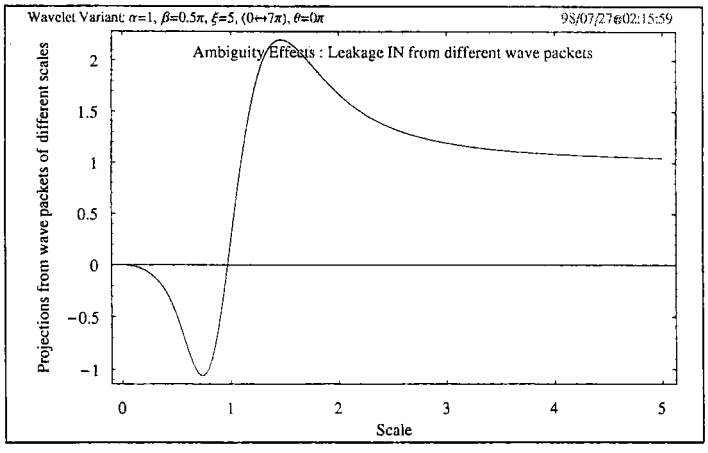

```
{1998, 7, 27, 2, 16, 49}    CPU:(00, 00, 9.72);    Time:(00, 00, 09)
```

■ Leakage in (Morlet)

```
(* ---------- Frequency Leakage In (Morlet) ---------- *)
typestr="Morlet Wavelet: ";
xlabel="Scale";
ylabel="Projections from wave packets of different scales";
flabel="Ambiguity Effects : Leakage IN from different wave packets";
<<"c:/lee/mat/000-pi_nb-m.m";
(*  There exists closed analytical form  *)
frelkginM[peakshiftv_, scav_, xlimitv_, phav_, xiv_] :=
   2 * Integrate[Cos[u/scav]*Cos[(u)]*
     Exp[-((u - peakshiftv)^2+ (u/scav)^2)/(2*xiv^2)],
     {u, 0, Infinity}
];
peakshiftpl=0;  peakshift= peakshiftpl * Pi;
xlimitpl=7;  xlimit=xlimitpl * Pi;
phapl=0;  pha=phapl * Pi;
xi=5;
scapl=1;
dofrelkginM=frelkginM [peakshift, sca, xlimit, pha, xi](*analytical form*)

datax= Table[ ni , {ni, 0.000, 5, 0.025}];
datay= Table[ N[dofrelkginM], {sca, 0.000 , 5 , 0.025 } ];
dataxy=Table[ {datax[[ i ]], datay[[i]]}, {i,1 ,Length[datax]}];
doshowxy;
```

$$2\,\text{If}\left[\text{Im}\left[\frac{1}{\text{sca}}\right] == 0 \;\&\&\; \text{Re}\left[\frac{1}{\text{sca}^2}\right] > -1 \;\&\&\; \text{Re}\left[\frac{1+\text{sca}^2}{\text{sca}^2}\right] > 0,\right.$$

$$\left.\frac{5\left(E^{-\frac{25(-1+\text{sca})^2}{2(1+\text{sca}^2)}} + E^{-\frac{25(1+\text{sca})^2}{2(1+\text{sca}^2)}}\right)\sqrt{\frac{\pi}{2}}\,\sqrt{1+\frac{1}{\text{sca}^2}}\,\text{sca}^2}{2\,(1+\text{sca}^2)},\ \int_0^\infty E^{\frac{1}{50}\left(-u^2-\frac{u^2}{\text{sca}^2}\right)}\,\text{Cos}[u]\,\text{Cos}\left[\frac{u}{\text{sca}}\right]\,du\right]$$

Ambiguity Effects : Leakage IN from different wave packets

Morlet Wavelet: α=1, β=0π, ξ=5, (0↔7π), θ=0π

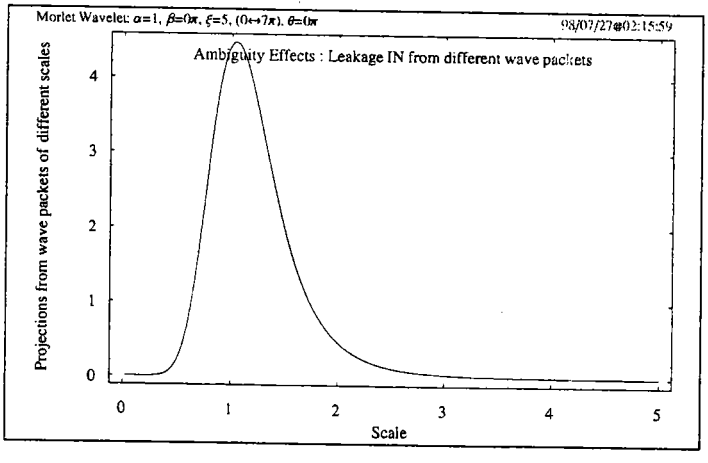


```
Graphics::gptn :
 Coordinate ComplexInfinity in {0., ComplexInfinity} is not a floating-point number.
```

```
{1998, 7, 27, 2, 16, 58}    CPU:(00, 00, 7.47);     Time:(00, 00, 08)
```

■ `<< "c:/lee/mat/000-p1_nb-m.m"`

```
FindMinimum[-1 * 10 *
  ((E^(-25 (-1+sca)^2/(2 (1+sca^2))) + E^(-25 (1+sca)^2/(2 (1+sca^2)))) Sqrt[Pi/2] Sqrt[1 + 1/sca^2] sca^2) / (2 (1 + sca^2)), {sca, 1.01}]
<< "c:/lee/mat/000-p2_nb-m.m"
{-4.47397, {sca → 1.03926}}
{1998, 7, 27, 2, 17, 6}    CPU:(00, 00, 0.05);     Time:(00, 00, 00)
```

■ Phase noise | File | Macro | LeakOut | LeakIn | PhaseNoise | Root | Others | End

■ **Phase noise (Wavelet variant)**

```
(* ---------- Phase Noise ---------- *)
typestr="Wavelet Variant: ";
xlabel="Phase";
ylabel="Projections from different phases";
flabel="Phase Noise : Related to differnet locations of a wave packet";
<<"c:/lee/mat/000-p1_nb-m.m";
integright[peakshiftv_, scaadjv_, xlimitv_, phav_, xiv_] :=
  NIntegrate[Cos[u/scaadjv-phav]*Sin[u]*
    Exp[-((u -peakshiftv )^2. + (u/scaadjv-phav)^2.)/(2*xiv^2)],
    {u, 0, xlimitv}
    , MinRecursion->3, MaxRecursion->10 ];
integleft[peakshiftv_, scaadjv_, xlimitv_, phav_, xiv_] :=
  NIntegrate[Cos[u/scaadjv-phav]*Sin[-u]*
    Exp[-((u + peakshiftv )^2. + (u/scaadjv-phav)^2.)/(2*xiv^2)],
    {u, -1.*xlimitv, 0}
    , MinRecursion->3, MaxRecursion->10 ];
peakshiftp1=0.5;  peakshift= peakshiftp1 * Pi;
xlimitp1=7;  xlimit=xlimitp1 * Pi;
phap1=0;  pha=phap1 * Pi;
xi=5;
scaadj= 0.969621557058245997;  scap1=scaadj;
phaintp1=Table[  integright[peakshift, scaadj, xlimit, phav, xi],
                 {phav, 0.05 Pi,  6.5  Pi , 0.05 Pi } ];
phaintp2=Table[  integleft[peakshift, scaadj, xlimit, phav, xi],
                 {phav, 0.05 Pi,  6.5  Pi , 0.05 Pi } ];
phaintmid=2 * Table[  integleft[peakshift, scaadj, xlimit, phav, xi],
                 {phav, 0.00 Pi,  0.00 Pi , 0.05 Pi } ];
posshiftsum=phaintp1+phaintp2;
midintsum=phaintmid;
datax=Join[ -1* Reverse[Table[ ni * Pi, {ni, 0.05, 6.5, 0.05}]], {0}, Table[
ni * Pi, {ni, 0.05, 6.5, 0.05}] ];
datay=Join[ Reverse[posshiftsum], midintsum, posshiftsum];
dataxy=Table[ {datax[[ i ]], datay[[i]]}, {i,1 ,Length[datax]}];
doshowxy;
```

```
Phase Noise : Related to differnet locations of a wave packet

Wavelet Variant: α=0.96962, β=0.5π, ξ=5, (0↔7π), Θ=0π
```

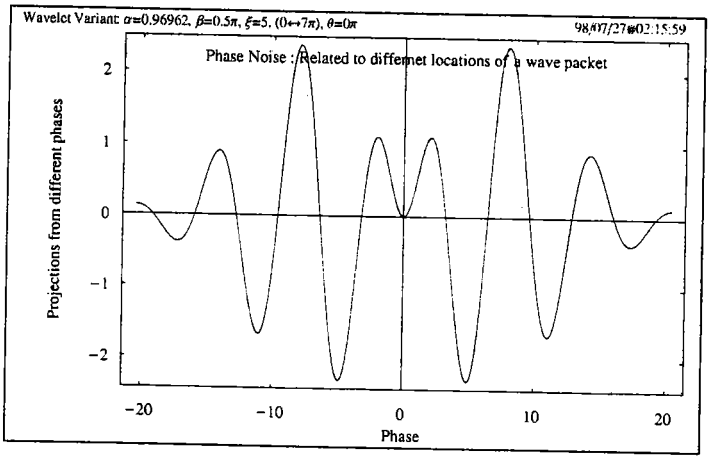

{1998, 7, 27, 2, 17, 6} CPU:(00, 00, 38.06); Time:(00, 00, 39)

■ Phase noise (Morlet)

```
(* ----------        Phase Noise (Morlet)        ---------- *)
typestr="Morlet Wavelet: ";
xlabel="Phase";
ylabel="Projections from different phases";
flabel="Phase Noise : Related to differnet locations of a wave packet";
<<"c:/lee/mat/000-p1_nb-m.m";
integrightM[peakshiftv_, scaadjv_, xlimitv_, phav_, xiv_] :=
  NIntegrate[Cos[u/scaadjv-phav]*Cos[u]*
    Exp[-((u -peakshiftv )^2. + (u/scaadjv-phav)^2.)/(2*xiv^2)],
    {u, 0, xlimitv}
    , MinRecursion->3, MaxRecursion->10 ];
integleftM[peakshiftv_, scaadjv_, xlimitv_, phav_, xiv_] :=
  NIntegrate[Cos[u/scaadjv-phav]*Cos[-u]*
    Exp[-((u + peakshiftv )^2. + (u/scaadjv-phav)^2.)/(2*xiv^2)],
    {u, -1.*xlimitv, 0}
    , MinRecursion->3, MaxRecursion->10 ];
peakshiftp1=0.0;  peakshift= peakshiftp1 * Pi;
xlimitp1=7;  xlimit=xlimitp1 * Pi;
phap1=0;  pha=phap1 * Pi;
xi=5;
scaadj= 1;
scap1=scaadj;
phaintp1=Table[  integrightM[peakshift, scaadj, xlimit, phav, xi],
                 {phav, 0.05 Pi,  6.50 Pi , 0.05 Pi } ];
phaintp2=Table[  integleftM[peakshift, scaadj, xlimit, phav, xi],
                 {phav, 0.05 Pi,  6.50 Pi , 0.05 Pi } ];
phaintmid=2 * Table[  integleftM[peakshift, scaadj, xlimit, phav, xi],
                 {phav, 0.00 Pi,  0.00 Pi , 0.05 Pi } ];
posshiftsum=phaintp1+phaintp2;
midintsum=phaintmid;
datax=Join[ -1* Reverse[Table[ ni * Pi, {ni, 0.05, 6.50, 0.05}]], {0},
Table[ ni * Pi, {ni, 0.05, 6.50, 0.05}] ];
datay=Join[ Reverse[posshiftsum], phaintmid, posshiftsum];
dataxy=Table[ {datax[[ i ]], datay[[i]]}, {i,1 ,Length[datax]}];
doshowxy;
```

Phase Noise : Related to differnet locations of a wave packet

Morlet Wavelet: α=1, β=0.π, ξ=5, (0↔7π), θ=0π

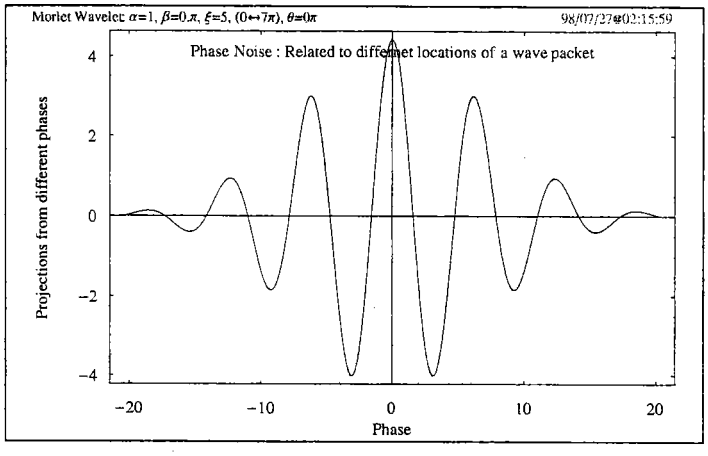

{1998, 7, 27, 2, 17, 45} CPU:(00, 00, 29.99); Time:(00, 00, 30)

Roots | File | Macro | LeakOut | LeakIn | PhaseNoise | Root | Others | End

```
<< "c:/lee/mat/000-p1_nb-m.m"
g[b_, a_, s_] := Integrate[Cos[u/a]*Sin[(u)]*
      Exp[-((u-Pi/2.)^2.+u^2.)/(2*s^2)], {u, 0, b}]
FindRoot[g[5.*Pi, a, 5] == 0, {a, 0.95, 0.7, 1.2}]
<< "c:/lee/mat/000-p2_nb-m.m"
```

{a → 0.970672}

{1998, 7, 27, 2, 18, 16} CPU:(00, 00, 44.27); Time:(00, 00, 44)

```
<< "c:/lee/mat/000-p1_nb-m.m"
g[b_, a_, s_] := Integrate[Cos[u/a]*Sin[(u)]*
      Exp[-((u-Pi/2.)^2.+u^2.)/(2*s^2)], {u, 0, b}]
FindRoot[g[7.*Pi, a, 5] == 0, {a, 0.9696, 0.7, 1.2}]
<< "c:/lee/mat/000-p2_nb-m.m"
```

{a → 0.970672}

{1998, 7, 27, 2, 19, 0} CPU:(00, 00, 44.71); Time:(00, 00, 45)

```
<< "c:/lee/mat/000-p1_nb-m.m"
g[b_, a_, s_] := Integrate[Cos[u/a]*Sin[(u)]*
      Exp[-((u-Pi/2.)^2.+(u/a)^2.)/(2*s^2)], {u, 0, b}]
FindRoot[g[5.*Pi, a, 5] == 0, {a, 0.97, 0.7, 1.2}]
<< "c:/lee/mat/000-p2_nb-m.m"
(* Run["mmawav.bat"]; *)
```

{a → 0.969622}

{1998, 7, 27, 2, 19, 46} CPU:(00, 01, 17.17); Time:(00, 01, 17)

Others | File | Macro | LeakOut | LeakIn | Phase Noise | Root | Others | End

Close form integrations

$$g2(b\_, a\_, s\_) = \int_0^\infty \cos\left(\frac{u}{a}\right) \sin(u)\, e^{-\frac{\left(\frac{u}{a}\right)^{2.}+u^2}{2s^2}}\, du$$

```
<< "c:/lee/mat/000-p1_nb-m.m"
g2[b_, a_, s_] = Integrate[Cos[u/a] * Sin[(u)] *
      Exp[-((u)^2. + (u/a)^2.)/(2*s^2)], {u, 0, Infinity}]
<< "c:/lee/mat/000-p2_nb-m.m"
```

$$\text{If}\left[\text{Im}\left(\frac{1}{a}\right) == 0 \bigwedge \text{Re}\left(\frac{\left(\frac{1}{a}\right)^2 + 1}{s^2}\right) > 0,\ \frac{1}{\left(\frac{\left(\frac{1}{a}\right)^2+1}{s^2}\right)^{0.5}} \left(0.5 \left(\sqrt{\frac{(1+\frac{1}{a})^2 s^2}{(\frac{1}{a})^2+1}}\ {}_1F_1\left(1.; \frac{3}{2}; -\frac{(1+\frac{1}{a})^2 s^2}{2((\frac{1}{a})^2+1)}\right) \text{sgn}\left(1+\frac{1}{a}\right) + \sqrt{\frac{(a-1)^2 s^2}{((\frac{1}{a})^2+1)a^2}}\ {}_1F_1\left(1.; \frac{3}{2}; -\frac{(a-1)^2 s^2}{2((\frac{1}{a})^2+1)a^2}\right) \text{sgn}\left(1-\frac{1}{a}\right)\right)\right),$$

$$\int_0^\infty e^{\frac{-\left(\frac{u}{a}\right)^2 - u^2}{2s^2}} \cos\left(\frac{u}{a}\right) \sin(u)\, du\Big]$$

{1998, 1, 10, 0, 15, 19} CPU:(00, 00, 15.17); Time:(00, 00, 15)

```
If[Im[1/a] == 0 && Re[(1 + (1/a)^2.)/s^2] > 0,
 (0.5 (Sqrt[((-1 + a)^2 s^2)/((1 + (1/a)^2.) a^2)] Hypergeometric1F1[1., 3/2, -((-1 + a)^2 s^2)/(2 (1 + (1/a)^2.) a^2)] Sign[1 - 1/a] +
    Sqrt[((1 + 1/a)^2 s^2)/(1 + (1/a)^2.)] Hypergeometric1F1[1., 3/2, -((1 + 1/a)^2 s^2)/(2 (1 + (1/a)^2.))] Sign[1 + 1/a]))/
  ((1 + (1/a)^2.)/s^2)^0.5,
 Integrate[E^((-u^2 - (u/a)^2.)/(2 s^2)) Cos[u/a] Sin[u], {u, 0, Infinity}]]
```

{1998, 7, 26, 17, 28, 31} CPU:(00, 00, 5.05); Time:(00, 00, 05)

```
<< "c:/lee/mat/000-p1_nb-m.m"
g3[b_, a_, s_] = Integrate[Cos[u/a] * Sin[(u)] *
      Exp[-((u - Pi/2.)^2. + (u/a)^2.)/(2*s^2)], {u, 0, Infinity}]
<< "c:/lee/mat/000-p2_nb-m.m"
```

$$\int_0^\infty E^{\frac{-(-1.570796+u)^2 - (\frac{u}{a})^{2.}}{2s^2}} \text{Cos}\left[\frac{u}{a}\right] \text{Sin}[u]\, du$$

{1998, 7, 27, 2, 21, 8} CPU:(00, 00, 8.79); Time:(00, 00, 09)

```
<< "c:/lee/mat/000-p1_nb-m.m"
g4[ a_, s_] := NIntegrate[Cos[u / a] * Sin[(u)] *
      Exp[-((u - Pi / 2.) ^2. + (u / a) ^2.) / (2 * s^2)], {u, 0, Infinity}]
g4[ 0.969621557058245997, 5]
<< "c:/lee/mat/000-p2_nb-m.m"
```

2.76365×10^{-6}

{1998, 7, 27, 2, 21, 17} CPU:(00, 00, 2.2); Time:(00, 00, 02)

File Macro PeakOut PeakIn PhaseNoise Root Coherence End

■ Appendix

The Unevaluatable

Chapter 4

Tests on Numerical Simulations and Wave Tank Signals

4.1 Numerical and experimental signals

Both numerically simulated and experimentally acquired signals are used to test the performance of the wavelet variant and the Morlet wavelet. Note again that all comparison pairs use the same parameters.

For numerical experimentation the following signals are used:

- A parabolic chirp with a frequency range of zero to Nyquist rate of 100 Hz;
- A signal composed of two liner chirps that have equal power and cross at a point of half Nyquist frequency (it is here called an X-signal);
- An X-signal with a power ratio 0.01 between component signals;
- A signal composed of two liner chirps that are parallel and have the same power content;
- A signal composed of two liner chirps that are parallel but with a power ratio of 0.04.

For test on experimental data, water wave signals generated by wind or mechanic wave generator in a laboratory wave tank are used. They include:

- Short wind waves of spectral peak of 2.0 to 2.6 Hz;
- Stokes waves of different fundamental harmonic frequencies and wave steepness.

4.2 Results and Discussions

- Figures 4.1, 4.2, and 4.3 show the zoom-in of a section of the parabolic chirp under several setups. The top two sub-figures in figure 4.1 are based on the modulus definition of equation 2.3; these time-frequency renditions are nearly identical to those of the Morlet wavelet. The bottom two sub-figures are associated with the wavelet variant transform, and the time-frequency modulus and phase maps are rendered in accordance with equations 2.4 and 2.5. It is quite clear that the current wavelet variant provides a much enjoyable and also easier way in identifying the locations of the instantaneous frequency. Moreover, it is hard to find any significant feature from the phase planes derived from the Morlet wavelet coefficients; on the contrary, the phase plane of the wavelet variant is just as informative as the corresponding modulus plane.
- Figure 4.2 also shows the same time-Frequency zoom-in, but here they are associated with different analyzing resolutions and also with different adaptations in its time-frequency windows (i.e., different ranges of ω_0). Even though here the discrete resolution in numerics is coarser when compared with the previous one and the resolution points might not fall exactly at those of instantaneous frequency, the phase plane still provides very clear features at all the interfacial resolution points. While in the mean time the modulus plane locates the exact matches between instantaneous frequencies and numerical resolution points.
- Figure 4.3 shows additionally the usefulness of the wavelet variant phase renditions. Through the use of phase rotations or different phase definitions, one sees from this figure as well as from the previous two figures that various important time-frequency features are glittered by the sharp contrast in phase. In addition the alternating phase strips are capable of showing the troughs or

peaks of a signal. One more point to note is that the contrasting phases are mostly seated at convenient phase separations.

- Figure 4.4 shows the whole parabolic chirp for both the Morlet wavelet and the wavelet variant. Again, the phase plane of the Morlet wavelet has far more unwanted features than anything that can be of practical significance. For the wavelet variant, note that there is a slight up-shift of instantaneous frequency when compared to that of an analytic Gabor transform. This up-shift factor is approximately $\frac{1}{0.9696}$.

- Figures 4.5 and 4.6 show time-frequency characterizations of an X-signal composed of two chirps of equal power using both the Morlet wavelet and the wavelet variant. These figures feature identical depictions as were provided by those of the parabolic chirp.

- 4.7 gives the distribution of the time-frequency resolutions for the X-signal using the wavelet variant. The middle sub-figure is done with a phase rotation. Here they basically show the effects of frequency leakage and phase noise. The saw-tooth shape peaks in the 3-D figure reflect the non-exact matching of instantaneous frequency and numerical resolution.

- Figure 4.8 shows the ridge extraction of a signal composed of a pair of parallel chirps of equal power. The frequency separation between the two chirps is one tenth of the Nyquist rate. The power ridge given by the Morlet wavelet is entirely misleading; while for the wavelet variant the two lines between the alternating dark band is mostly identifiable except near the Nyquist frequency (top right sub-figure) and the two lines are represented by the two sharp peaks in the 3-D plot (bottom right sub-figure, where the rendering is inverted, i.e., a trough in the 2-D plane turns to a peak in the 3-D figure). Quite obviously, the devised wavelet variant provides a much easier and unambiguous identification of the two component chirps.

- Figure 4.9 shows the ridge extraction of a signal composed of a pair of parallel chirps with difference in their power contents (a ratio of 0.04) using both the Morlet wavelet and the wavelet variant. Figure 4.10 shows the time-frequency phase planes for an X-signal with power ratio of 0.01 between component

chirps using the Morlet wavelet (top sub-figure) and the wavelet variant (bottom sub-figure). In general, both transforms show difficulty in differentiating such a large power difference for the two nearby instantaneous frequencies. The weak component signal has been overshadowed by contamination. Nevertheless, the wavelet variant phase plane is still a bit more informative.

- Figure 4.11 shows time-frequency features of a water wave signal measured in a wind blowing laboratory tank using the Morlet wavelet (left sub-figures) and the wavelet variant (right sub-figures). Figure 4.12 shows the wavelet variant time-frequency planes for a less developed water wave of small wind speed (i.e., with a spectral peak located at higher frequency). Still the wavelet variant yields better and easier identifications of instantaneous frequencies from both modulus and phase representations. Besides, from the phase planes of the wavelet variant one seems more likely to get an idea of where the higher frequency ridge points locate.

- Figure 4.13 shows time-frequency features of a mechanically generated Stokes wave using the Morlet wavelet (left sub-figures) and the wavelet variant (right sub-figures). Again, the wavelet variant has obvious advantages over the Morlet wavelet in identifying time-frequency features from both modulus and phase representations. Interestingly, there might also be an indication of the Benjamin-Feir side-band instability [1, 2, 31, 10, 12, 11, 19, 20, 9, 27, 24, 25, 17] at the second harmonic band as is evidenced by the rapidly oscillating interfacial points in the phase plane based on the wavelet variant.

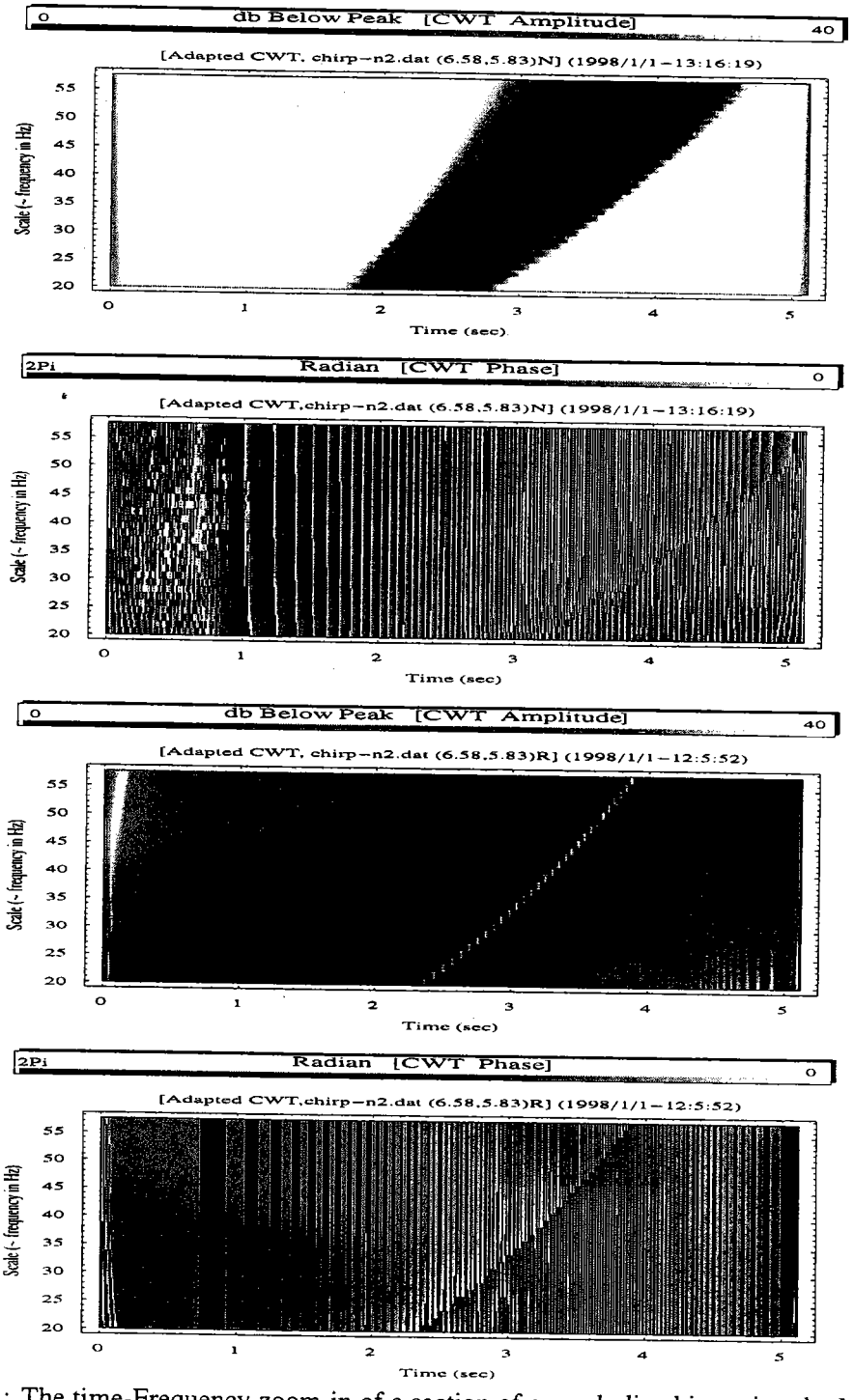

Figure 4.1: The time-Frequency zoom-in of a section of a parabolic chirp using the Morlet wavelet and the wavelet variant. The top two sub-figures are based on the modulus definition of equation 2.3; therefore, they are almost identical to those of the Morlet wavelet. The bottom two sub-figures are associated with the wavelet variant based on equations 2.4 and 2.5. Various implications are stated in the text.

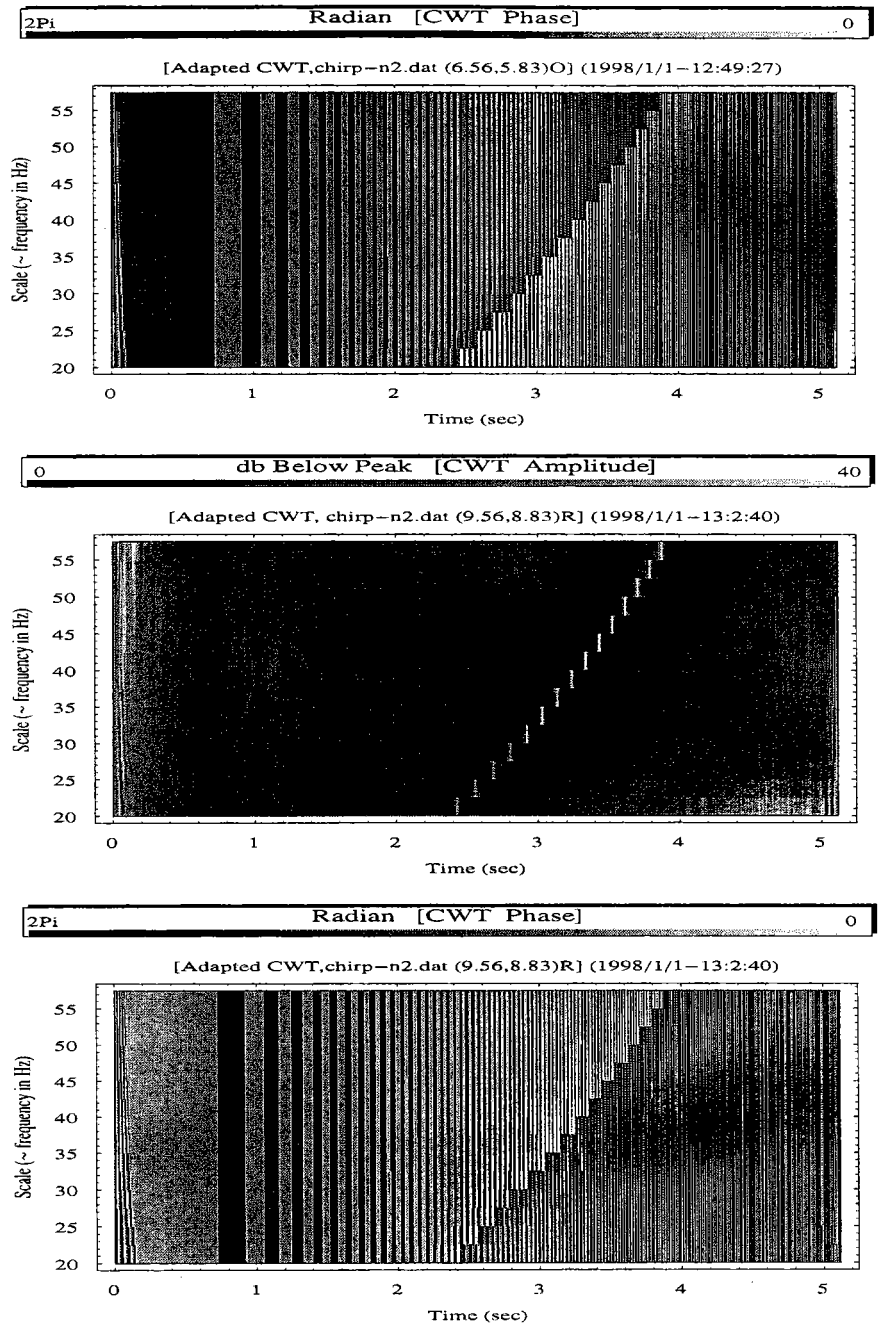

Figure 4.2: The same time-Frequency zoom-in of a section of a parabolic chirp using the wavelet variant. Here the adaptations of time frequency windows and the discrete step (numerical resolution) are different from the previous ones. Even though the discrete resolution is coarser now, the phase plane still provides the same clear contrast at all the interfacial points; while the modulus plane locates the exact matches between instantaneous frequencies and numerical resolution points.

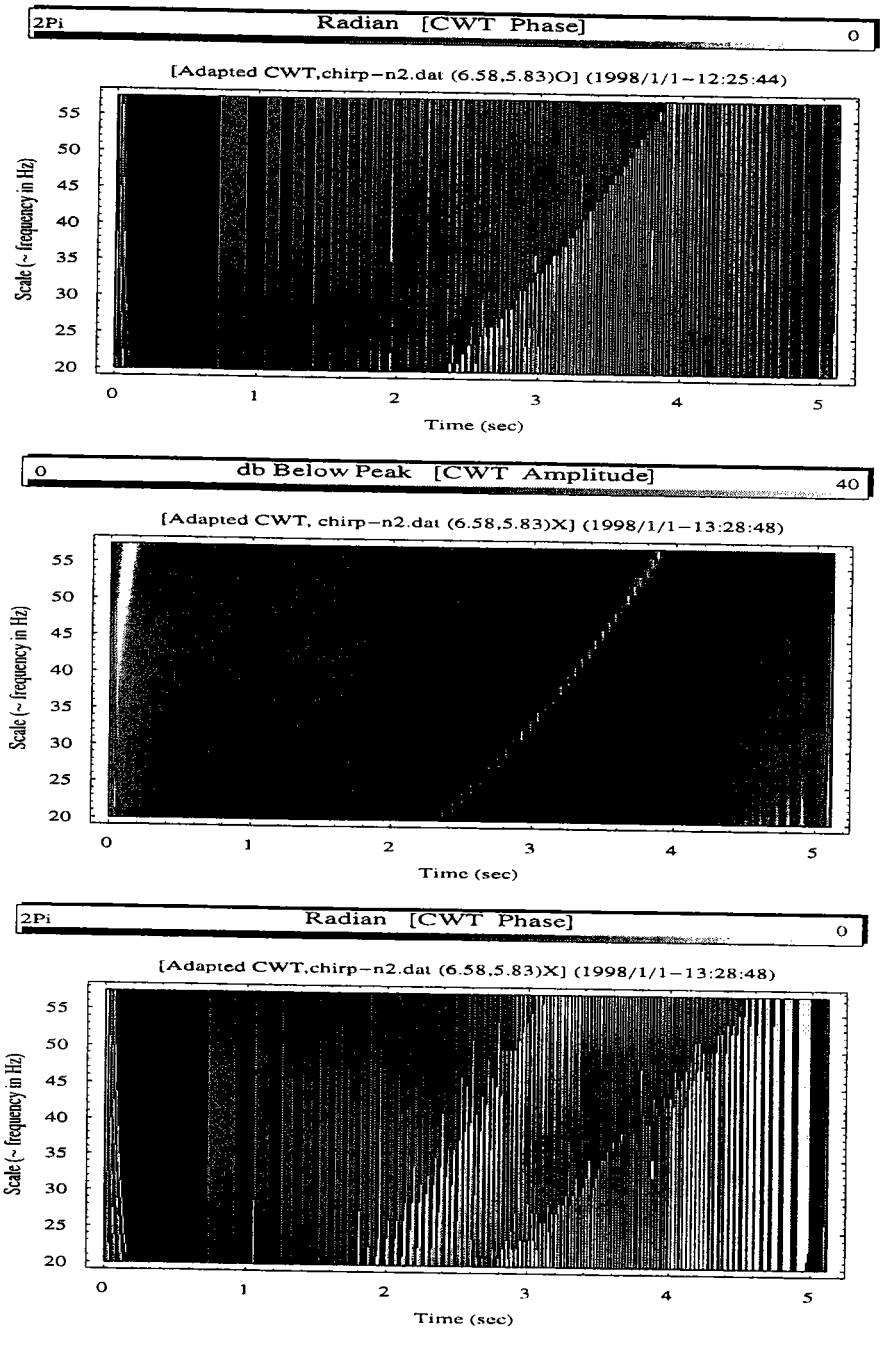

Figure 4.3: The time-Frequency zoom-in of a section of a parabolic chirp – effects of phase rotations. Combined with the two previous figures one sees that time-frequency characterizations are featured by the glittering of sharp contrast in phase. In addition, various contrasting phases are seated at convenient phase separations.

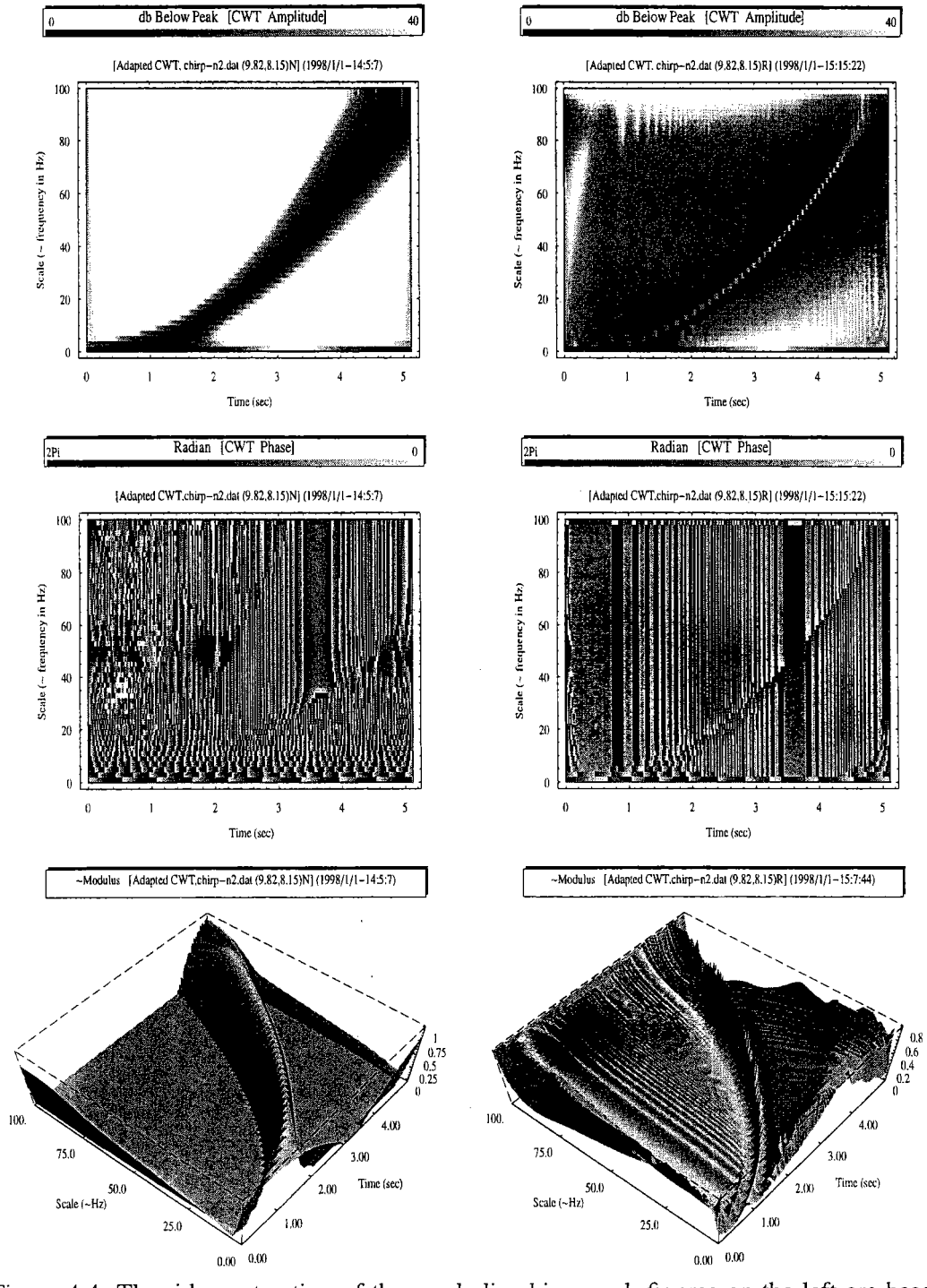

Figure 4.4: The ridge extraction of the parabolic chirp – sub-figures on the left are based on the Morlet wavelet basis; sub-figures on the right are associated with the wavelet variant. Again, the phase plane from the Morlet wavelet has far more unwanted features than anything that can be of practical interest. Note, for the wavelet variant, the frequency of the featuring curve is about $\frac{1}{0.9696}$ of that of the analytic Gabor transform.

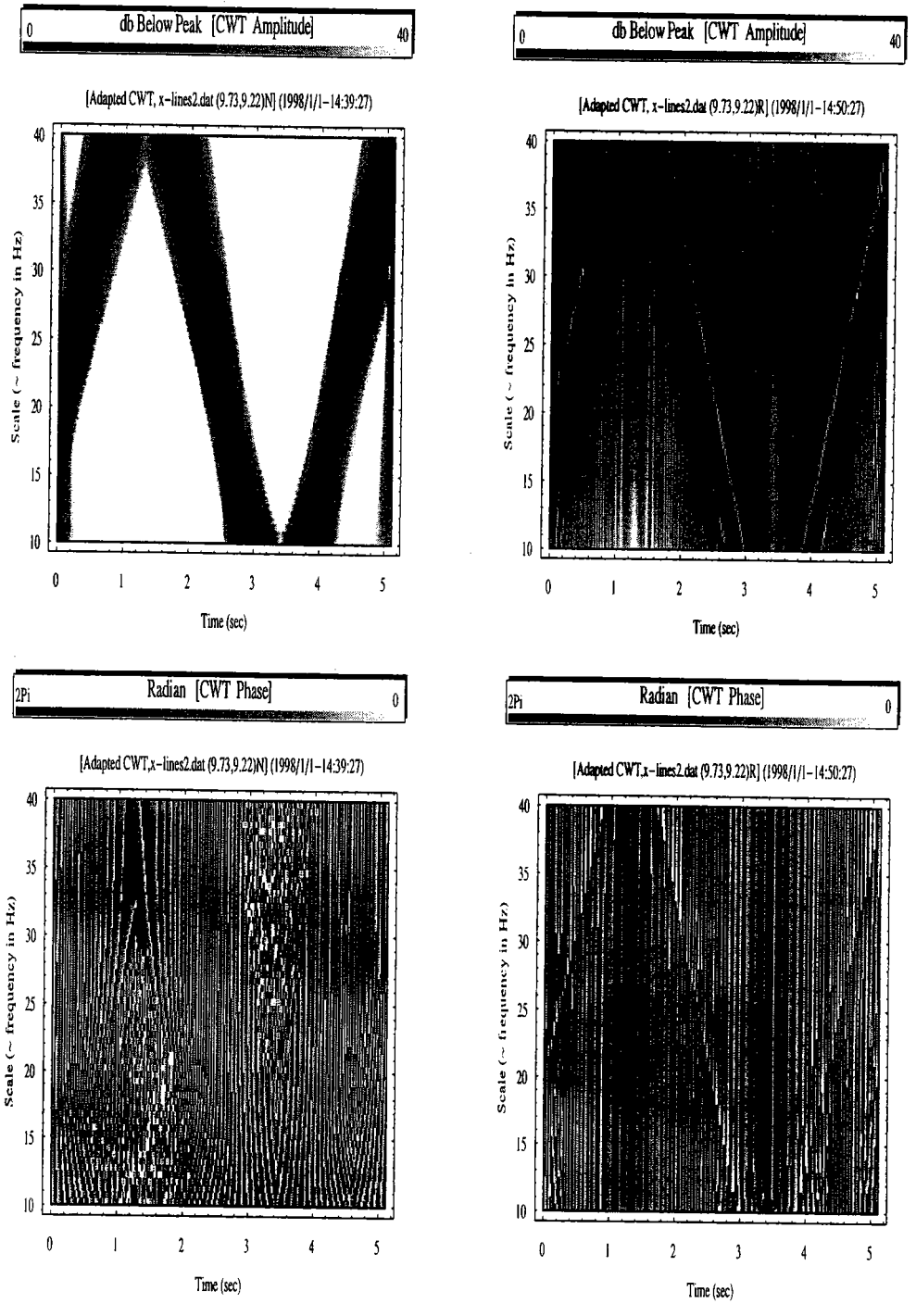

Figure 4.5: The Zoom-in of the ridge extraction of an X-signal composed of two crossing linear chirps of equal power. The sub-figures on the left are based on the Morlet wavelet basis; the sub-figures on the right are associated with the wavelet variant.

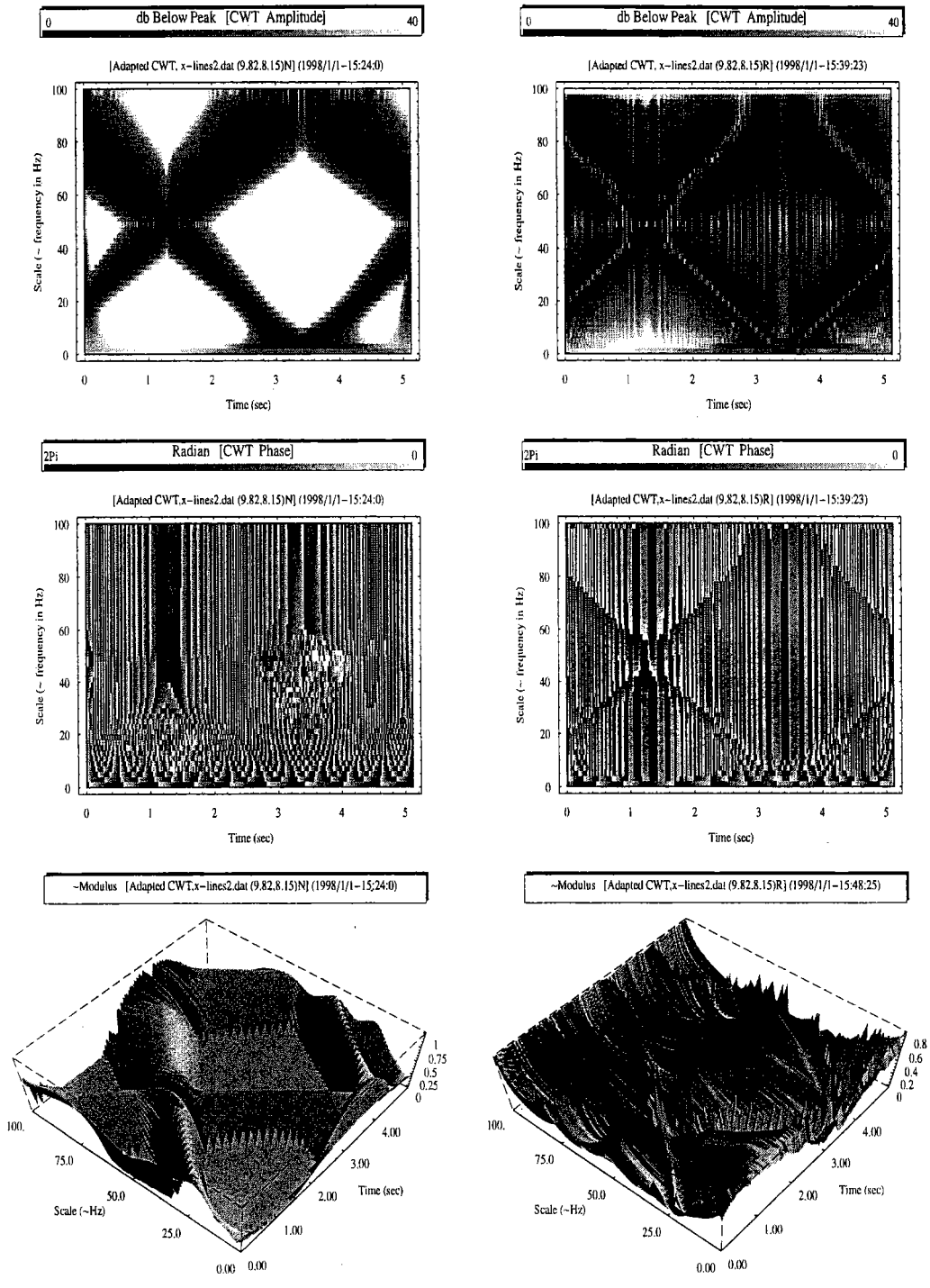

Figure 4.6: The ridge extraction of the X-signal using the Morlet wavelet (the sub-figures on the left) and the basis of the wavelet variant (the sub-figures on the right). Here the figures feature identical depictions as were provided by those of the parabolic chirp. The saw-tooth shapes of the right 3-D plot reflect the non-perfect match due to a coarser numerical resolution.

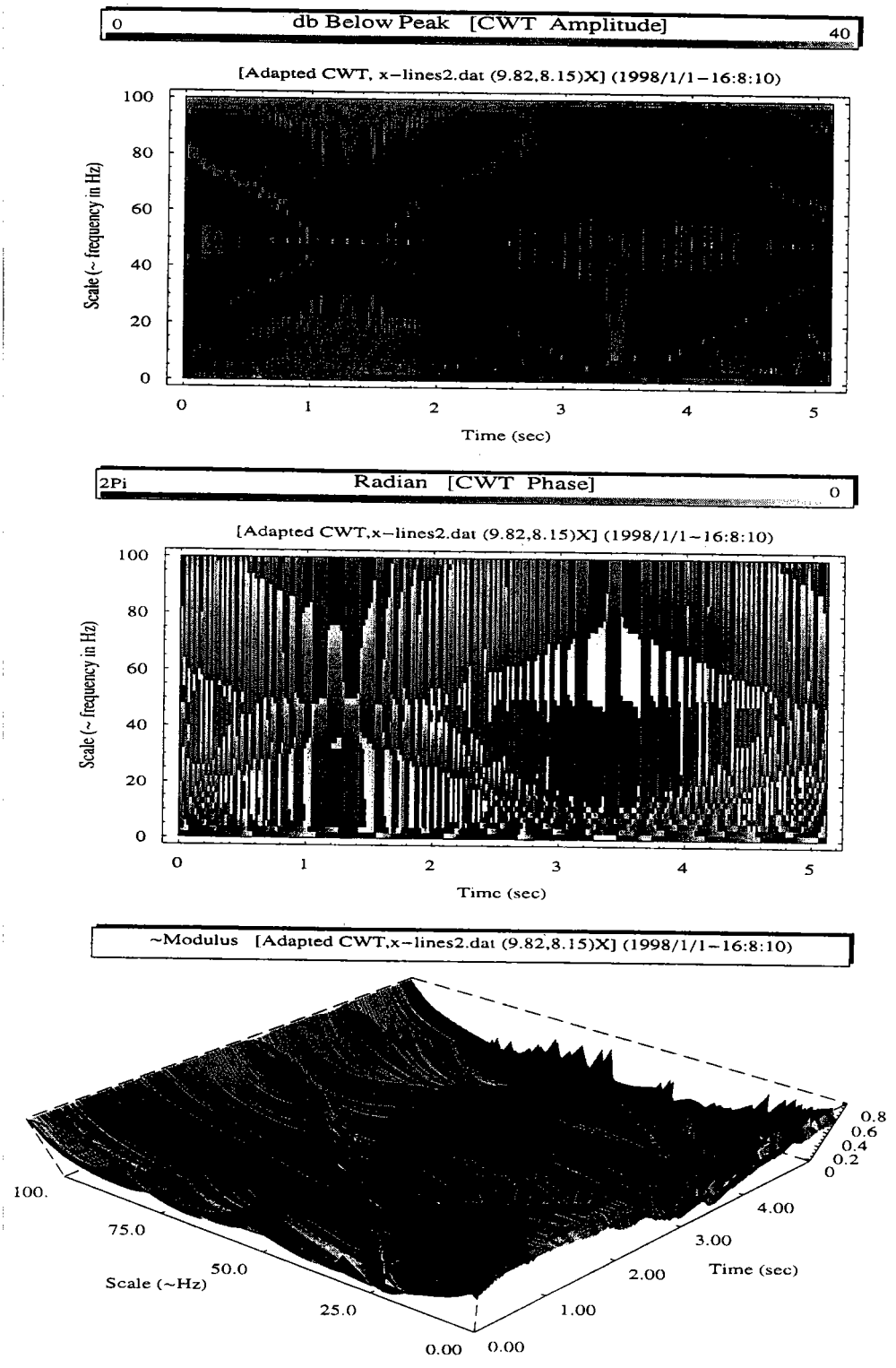

Figure 4.7: Ridge extraction of the X-signal using the wavelet variant with phase rotation – noting the capability of detecting the frequency leakage from the phase plane (the middle sub-figure).

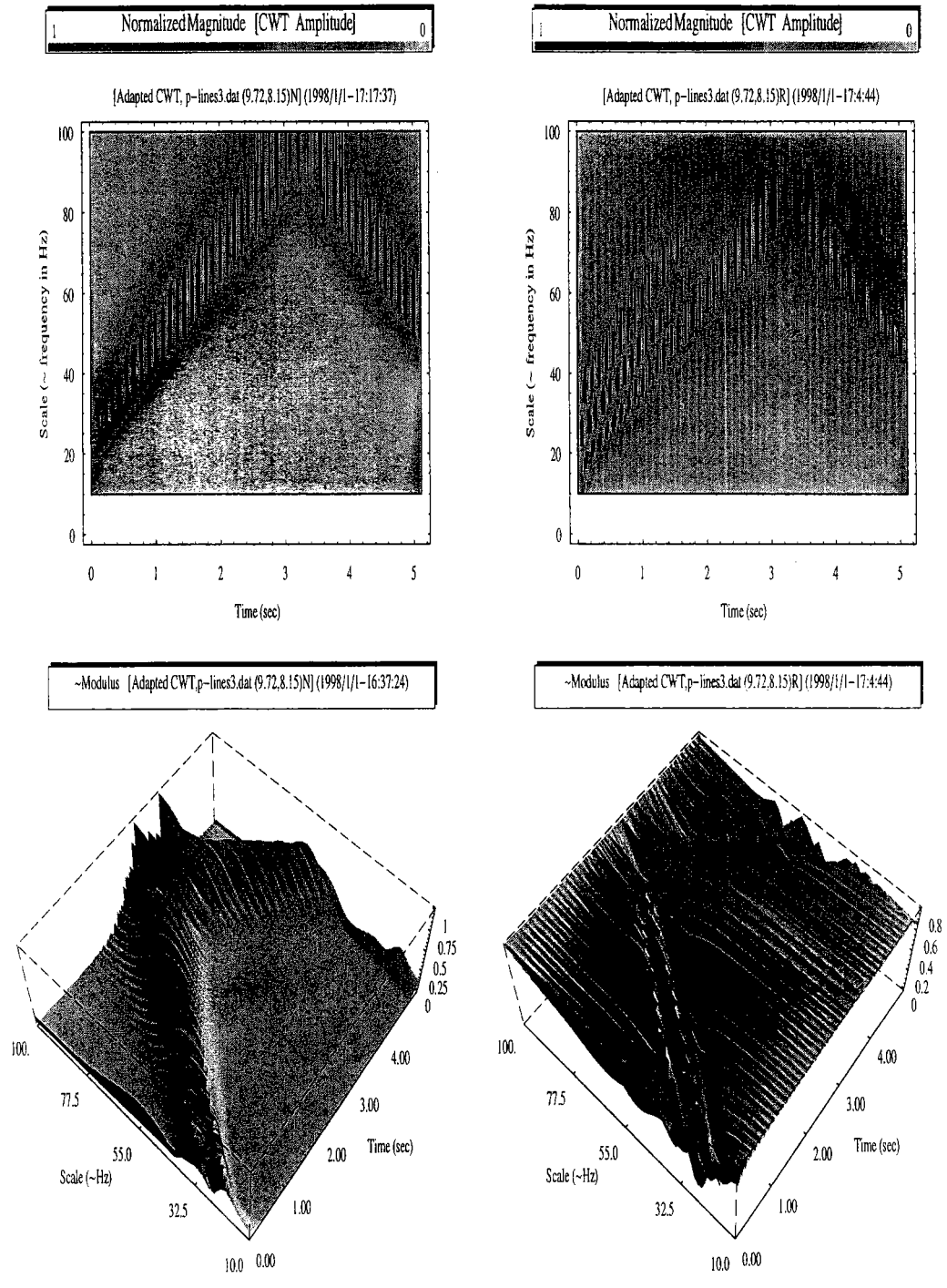

Figure 4.8: The ridge extraction of a signal composed of a pair of parallel chirps of equal power. The figures on the left are based on the Morlet wavelet basis; the figures on the right are associated with the wavelet variant basis – noting the much easier and unambiguous identification of the two component chirps when the devised wavelet variant is used.

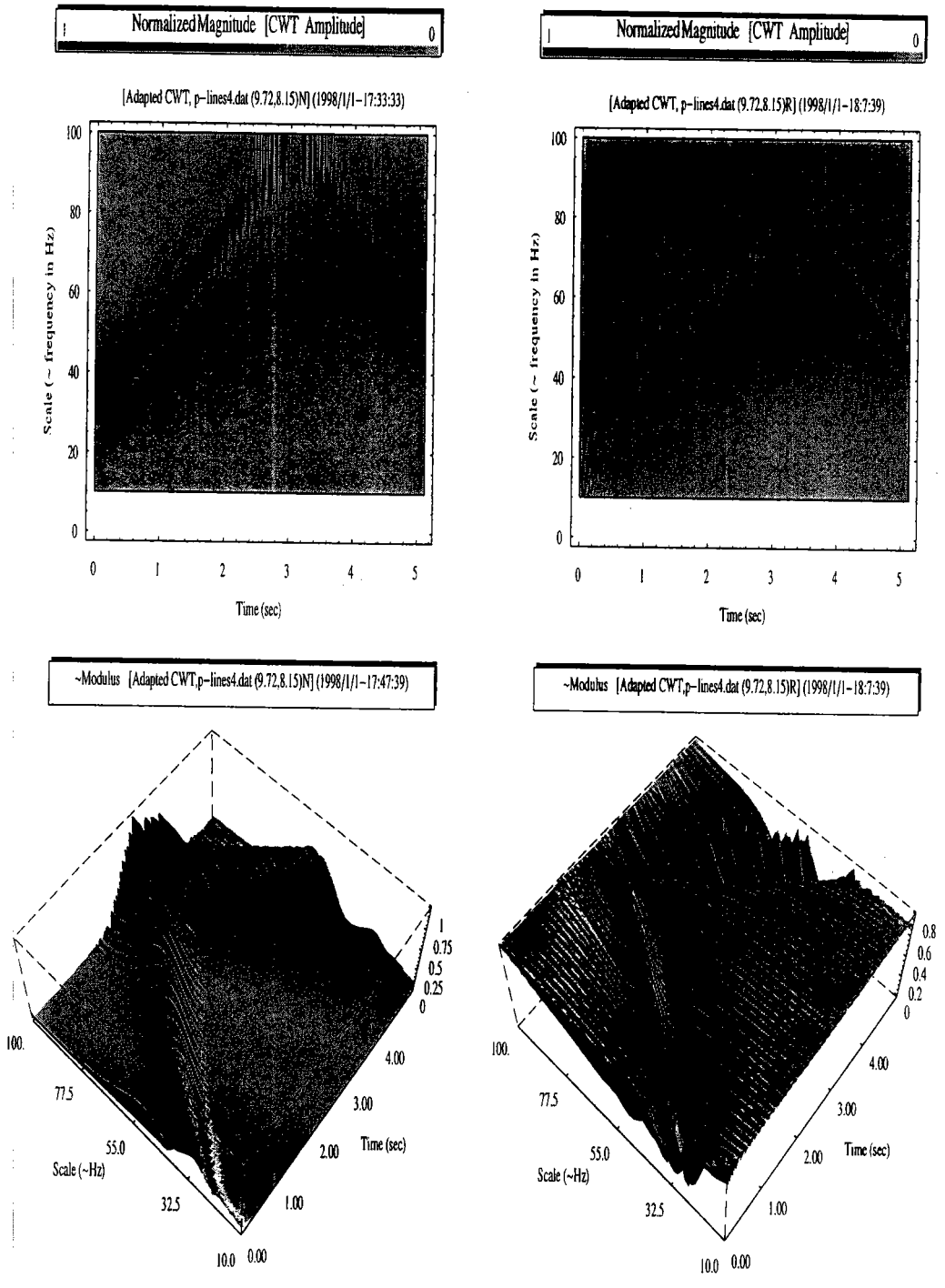

Figure 4.9: The ridge extraction of a signal composed of a pair of parallel chirps with significant difference in their power contents. The figures on the left are based on the Morlet wavelet; the figures on the right are associated with the wavelet variant. Here both transforms show difficulty in differentiating such a large power difference. The weak component signal has been overshadowed by ambiguity effects.

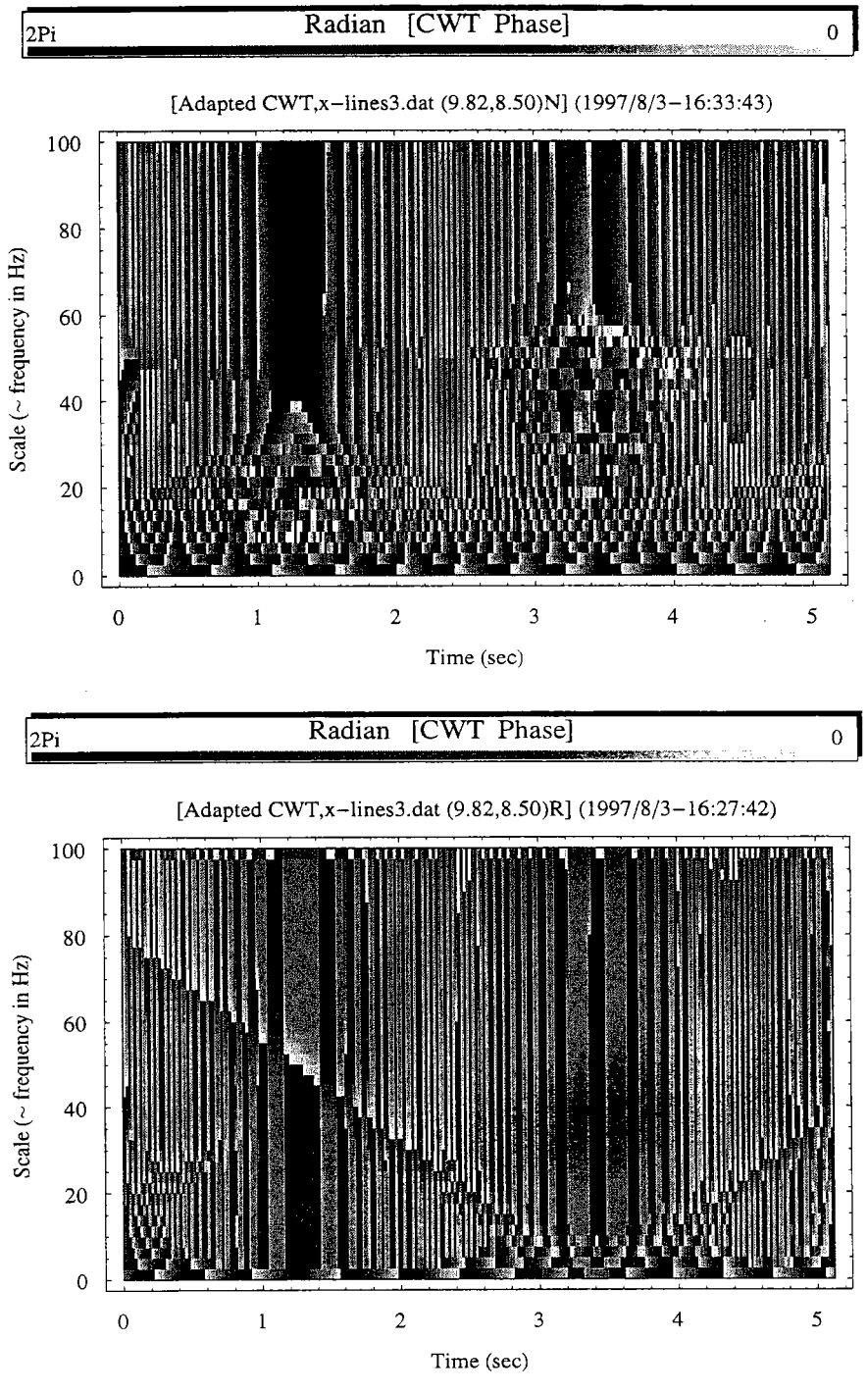

Figure 4.10: The time-frequency phase planes for an X-signal with a power ratio of 0.01 between component chirps using the Morlet wavelet (top sub-figure) and the wavelet variant (bottom sub-figure). The wavelet variant is still a bit more informative in identifying the weak signal.

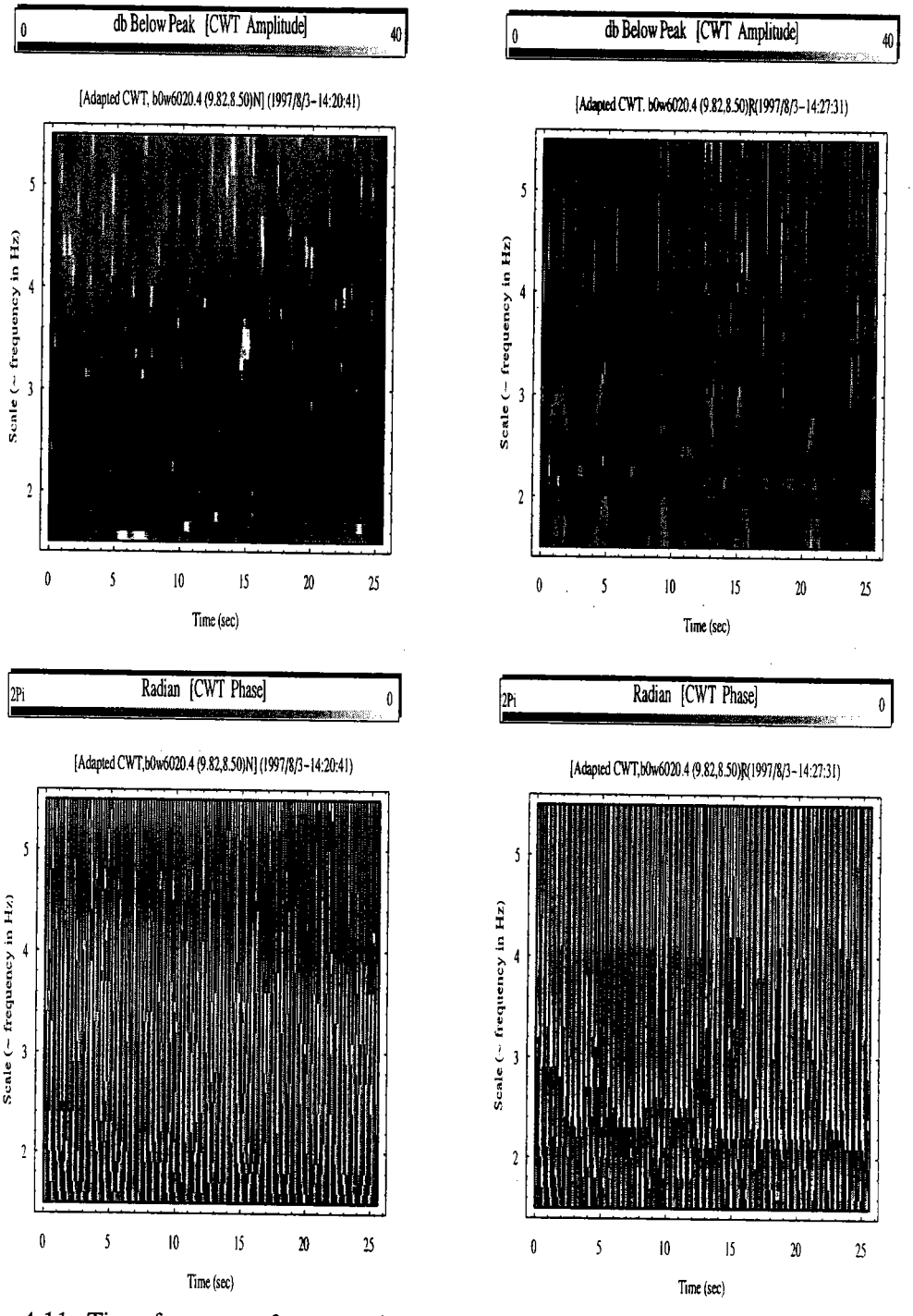

Figure 4.11: Time-frequency features of a water wave signal measured in a wind blowing laboratory tank using the Morlet wavelet (left sub-figures) and the wavelet variant (right sub-figures). The wavelet variant yields better identifications of instantaneous frequencies in both planes. Besides, the phase plane of the wavelet variant seems to be able to locate higher frequency ridge points.

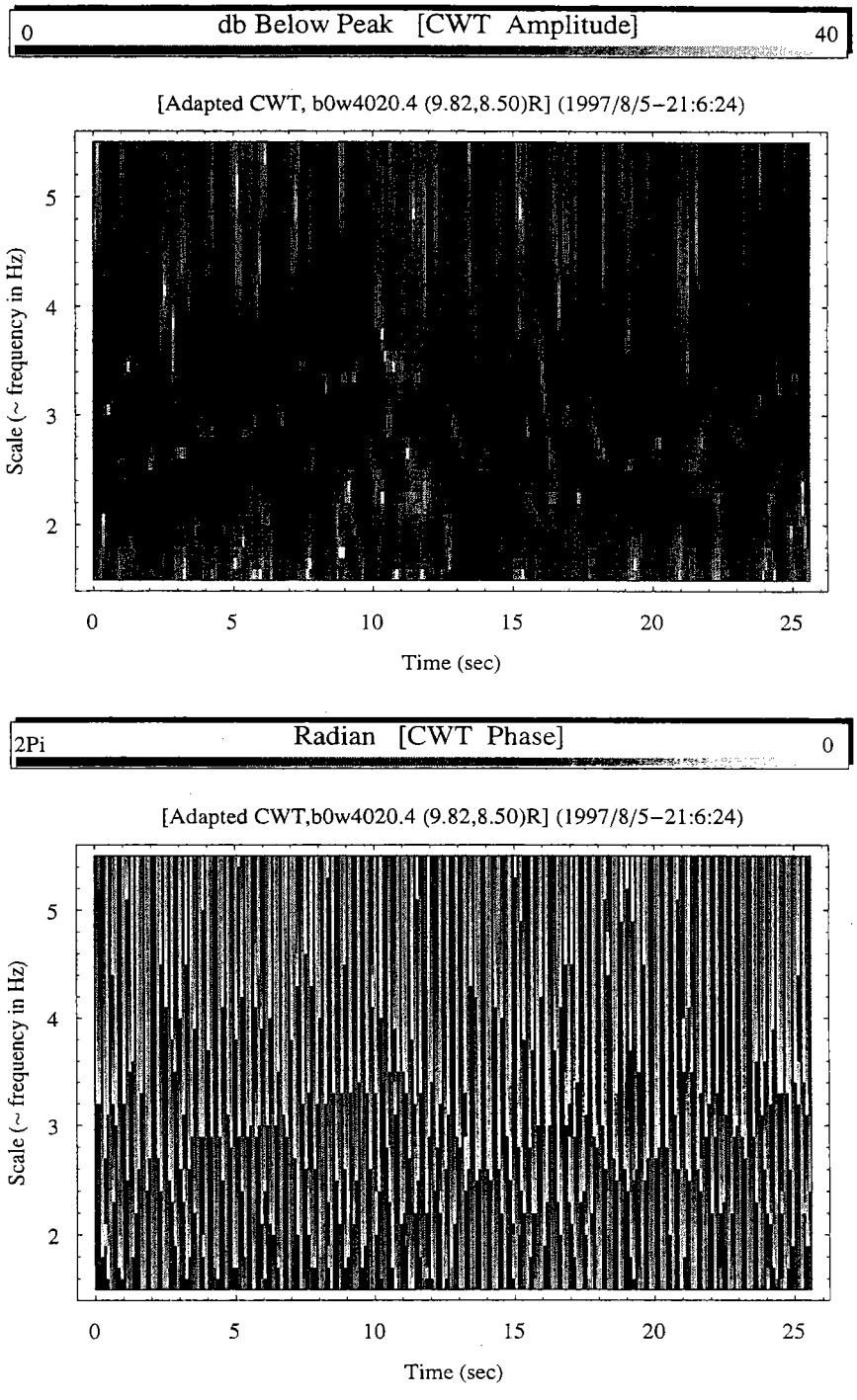

Figure 4.12: The wavelet variant time-frequency planes for a less developed water wave related to a smaller wind speed (i.e., with a spectral peak located at a higher frequency than the one associated with the previous figure).

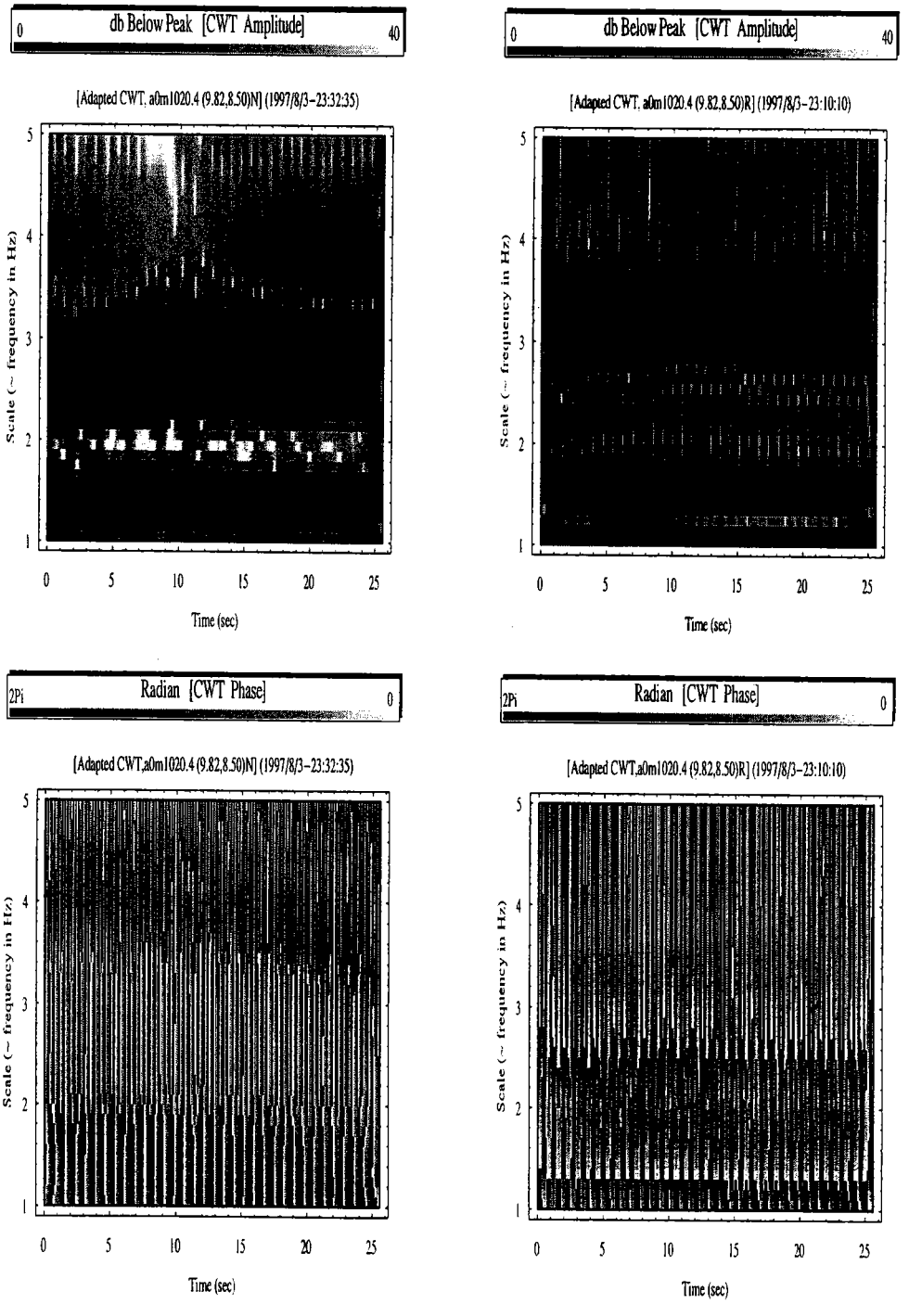

Figure 4.13: The identification of instantaneous frequencies of a Stokes wave using the Morlet wavelet (left sub-figures) and the wavelet variant (right sub-figures). As is evident, the wavelet variant provide easier and more precise identifications. And there might be also an indication of the side-band instability at the second harmonic band as is clearly evidenced from the wavelet variant phase plane.

Chapter 5

Conclusions

A wavelet variant as well as its associated time-frequency rendering methods are devised. The reasons that lead to the usefulness of the wavelet variant are illustrated through the characterizations of the projections of wave packets of different scales and phases into the wavelet variant, or vice versa. With reference to the Morlet wavelet in association with a continuous wavelet transform, we show that the present quasi-wavelet provides easier and clearer identifications of instantaneous frequencies using either the modulus or phase time-frequency plane. Most profoundly, the phase plane of the wavelet variant provides far more informative highlights for various featuring elements – such as ridge points, extends of frequency leakage and phase noise, the oscillating position of trough or peak of a component signal, and better indication of high frequency constituents.

REFERENCES

[1] Brooke Benjamin, T. Instability of periodic wave trains in nonlinear dispersive systems. *Proc. Roy. Soc. Lond.*, A299:59–75, 1967.

[2] Brooke Benjamin, T., and J. E. Feir. The disintegration of wave trains on deep water. *J. Fluid Mech.*, 27:417–430, 1967.

[3] Chui, C. K. *An Introduction to Wavelets*. Academic Press, Inc., San Diego, California, USA, 1992.

[4] Chui, C.K. On cardinal spline-wavelets. In M. B. Ruskai, G. Beylkin, R. Coifman, I. Daubechies, S. Mallat, Y. Meyer, and L. Raphael, editor, *Wavelets and Their Applications*, pages 439–452. Jones and Bartlett Publishers, Boston, New York, USA, 1992.

[5] Cohen, L. *Time-Frequency Analysis*. Prentice Hall PTR, Englewood Cliffs, New Jersey, USA, 1995.

[6] Daubechies, I. *Ten Lectures on Wavelets*. SIAM, Philadelphia, USA, 1992.

[7] Gabor, D. Theory of communication. *Journal of the IEE*, 93:429–457, 1978.

[8] Greenberg, M.D. *Advanced Engineering Mathematics*. Prentice Hall PTR, Englewood Cliffs, New Jersey, USA, 1988.

[9] Hwang, P. A, D. Xu, and J. Wu. Breaking of wind-generated waves: measurements and characteristics. *J. Fluid Mech.*, 202:177–200, 1989.

[10] Lake, B.M., and H.C. Yuen. A note on some nonlinear water wave experiments and comparison of data with theory. *J. Fluid Mech.*, 83:75–81, 1977.

[11] Lake, B.M., and H.C. Yuen. A new model for nonlinear gravity waves, part 1, physical model and experimental evidence. *J. Fluid Mech.*, 88:33–62, 1978.

[12] Lake, B.M., H.C. Yuen, H. Rundgaldier, and W.E. Ferguson. Nonlinear deep-water waves: Theory and experiment, part 2, evolution of a continuous wave train. *J. Fluid Mech.*, 83:49–74, 1977.

[13] Lee, Y.R. Signal analysis from wave modulation perspective – Part I: Characterizing the analytic signal procedure. Technical report, No.1997–7, Institute of Harbor and Marine Technology, Taichung, Taiwan, 1997.

[14] Lee, Y.R. The serach of the most appropriate function basis for laboratory water waves. Technical report, No.1998–5(II) Institute of Harbor and Marine Technology, Taichung, Taiwan, 1998.

[15] Lee, Y.R., and J. Wu. Continuous wavelet transform using a locally adapted time-frequency window. In *Proc. 18th Conf. on Coastal Engineering in Taiwan*, pages 95–106, 1996.

[16] Lee, Y.R., and J. Wu. Wavelet and wavelet packet best basis for laboratory water waves. In *Proc. 18th Conf. On Coastal Engineering in Taiwan*, pages 83–94, 1996.

[17] Lee, Y.R., and J. Wu. Time-frequency features and side band instability. In *Proc. 19th Conf. On Coastal Engineering in Taiwan*, pages 32–39, 1997.

[18] Lee, Y.R., and J. Wu. Wavelet coherences based on an optimum analyzing function basis. *Proc. 20th Conf. on Coastal Engineering in Taiwan*, pages 109–116, 1998.

[19] Longuet-Higgins, M.S. The instability of gravity waves of finite amplitude in deep water I, Superharmonics. *Proc. Roy. Soc. Lond.*, A360:471–488, 1978.

[20] Longuet-Higgins, M.S. The instability of gravity waves of finite amplitude in deep water II, Subharmonics. *Proc. Roy. Soc. Lond.*, A360:489–505, 1978.

[21] M. B. Ruskai, G. Beylkin, R. Coifman, I. Daubechies, S. Mallat, Y. Meyer, and L. Raphael, editor. *Wavelets and Their Applications*. Jones and Bartlett Publishers, Boston, New York, USA, 1992.

[22] Mallat, S. *A Wavelet Tour of Signal Processing*. Academic Press, Inc., San Diego, California, USA, 1998.

[23] Mallat, S., and S. Zhong. Wavelet transform maxima and multiscale edges. In M. B. Ruskai, G. Beylkin, R. Coifman, I. Daubechies, S. Mallat, Y. Meyer, and L. Raphael, editor, *Wavelets and Their Applications*, pages 67–104. Jones and Bartlett Publishers, Boston, New York, USA, 1992.

[24] Melville, W. K. The instability and breaking of deep water waves. *J. Fluid Mech.*, 115:165–185, 1982.

[25] Melville, W. K. Wave modulation and breakdown. *J. Fluid Mech.*, 128:489–506, 1983.

[26] Meyer, Y. *Wavelets and operators*. Cambridge University Press, New York, USA, 1992.

[27] Su, M.Y. Evolution of groups of gravity waves with moderate to high steepness. *Phys. Fluids*, 25:2167–2174, 1982.

[28] Tchamitchian, Ph., and B. Torresani. Ridge and skeleton extraction from the wavelet transform. In M. B. Ruskai, G. Beylkin, R. Coifman, I. Daubechies, S. Mallat, Y. Meyer, and L. Raphael, editor, *Wavelets and Their Applications*, pages 123–151. Jones and Bartlett Publishers, Boston, New York, USA, 1992.

[29] Wickerhauser, M.V. Acoustic signal compression with wavelet packets. In C.K. Chui, editor, *Wavelets: A tutorial in Theory and Applications*, pages 679–700. Academic Press, Inc., San Diego, California, USA, 1992.

[30] Wickerhauser, M.V. Comparison of picture compression methords: wavelet, wavelet packet, and local cosine. In C. K. Chui, editor, *Wavelets: Theory, Algorithms, and Applications*, pages 585–621. Academic Press, Inc., San Diego, California, USA, 1994.

[31] Yuen, H. C., and B. M. Lake. Nonlinear deep water waves: Theory and experiment. *Phys. Fluids*, 18:956–960, 1975.

Yueon-Ron Lee 李勇榮 (中縣 梧棲鎮 港研所)
Institute of Harbor and Marine Technology
83 Lin-Hai Rd., Wuchi, Taichung 43501
Taiwan

Voice & Fax:886-4-6564216 ext.417 ◇◇◇ Fax:886-4-6571329
Email: ronlee@ms4.hinet.net